Euro. Jnl of Applied Mathematics (1998), *vol.* 9, *pp.* 129–158. Printed in the United Kingdom

Diffraction by slender bodies

J. C. ENGINEER, J. R. KING and R. H. TEW

Department of Theoretical Mechanics, University of Nottingham, Nottingham NG7 2RD, UK

(*Received 4 April 1997; revised 10 December 1997*)

The scattering of high-frequency sound waves by two-dimensional curved boundaries has received much attention over the past few decades, with particular interest in the effects of tangential ray incidence. In the event that the radius of curvature is not small, an analysis near the point of tangency gives rise to the Fock–Leontovič equation for the local field amplitude which, in turn, matches the creeping field of Keller's geometrical theory of diffraction. If the radius of curvature is sufficiently small, however, then this analysis is not valid and it is necessary to solve the *full* Helmholtz equation in the presence of a parabolic boundary. Under these conditions, which are canonical for diffraction by a sufficiently slender body, results are presented for the case of a plane wave impinging upon an acoustically hard parabolic cylinder. This diffraction process engenders a creeping field at one tip of the slender body, which then propagates around the body to the other tip. Here its energy is partially reflected, partially transmitted and partially radiated out in a detached field. A full description of this is given, along with a discussion of the 'blunt' limit in which we show that not only do we get the traditional creeping field of Keller's geometrical theory of diffraction, but also an exponentially small backward-propagating creeping field not predicted by traditional ray methods.

1 Introduction

In this paper, we examine the two-dimensional scattering of a time-harmonic, scalar wave-field by an arbitrary finite, convex body in the high-frequency limit. The wave function might be the acoustic velocity potential for a compressible fluid surrounding the obstacle or perhaps a potential for an electromagnetic field. We adopt a Neumann boundary condition on the resulting Helmholtz equation, though other boundary conditions can also be examined using our methodology.

The principal tool for an asymptotic study of such a short-wavelength diffraction problem is ray theory and an account of its derivation and reviews of some examples are given by Keller & Lewis [1] and Babič & Buldyrev [2]. Essentially, the scattered field is expressed in terms of an amplitude and a phase, with the latter being a solution of the eikonal equation $\nabla u \cdot \nabla u = 1$. The characteristics of this partial differential equation yield the 'rays' along which we are able to construct and solve a recursive system of ordinary differential equations for successive amplitude terms in an expansion in reciprocal powers of wavenumber. This procedure can be applied at points of specular reflection when the local normal to the boundary bisects the angle between the incident and reflected rays (i.e. Snell's law is satisfied) and the local amplitude of the reflected ray is governed by the plane wave reflection coefficient, giving the initial condition for the leading order amplitude equation to provide the solution away from the boundary. This approach

cannot, however, be followed at points of diffraction, including points of non-analyticity of the boundary, such as a sharp edge, or points where the incoming ray and the reflecting boundary are tangent to one another.

In the case of a sharp edge, the appropriate inner problem near the tip is that of scattering by a half-plane, first analysed by Sommerfeld [3] and reviewed by Bowman *et al.* [4]. As is very well-known, this produces an expansion fan of diffracted rays centred on the edge, with a far-field amplitude that is dependent upon the local polar angle θ through a diffraction coefficient or 'directivity' function and which decays in an inverse square root fashion with the distance r from the tip. In precise terms, for a plane wave $e^{ik(x\cos\theta_i + y\sin\theta_i) - i\omega t}$ incident upon a rigid semi-infinite plane $y = 0, x > 0$, the tip-diffracted field is given by

$$\phi^{(d)}(r,\theta) \sim e^{ikr + \frac{i\pi}{4}} \sqrt{\frac{2}{\pi kr}} \frac{\sin\frac{1}{2}\theta_i \cos\frac{1}{2}\theta}{(\cos\theta - \cos\theta_i)} \quad \text{as} \quad k \to \infty, \tag{1.1}$$

to leading order, where θ_i is the angle of incidence of the incoming plane wave with respect to the half-plane, k is the wavenumber, $x = r\cos\theta$ and $y = r\sin\theta$. Of course, this expression is not uniform in θ and the solution must be modified near the critical directions $\theta = \theta_i, 2\pi - \theta_i$, which represent the boundaries for the regions occupied by the incident and reflected ray fields.

The case of tangency on a blunt body is more complicated; if the curvature κ_0 of the body at the point of tangency is much less than k, the appropriate scalings for the local arclength s and normal coordinate n are

$$s = \kappa_0^{-\frac{2}{3}} k^{-\frac{1}{3}} \hat{s}, \quad n = \kappa_0^{-\frac{1}{3}} k^{-\frac{2}{3}} \hat{n}, \tag{1.2}$$

where $\hat{s}$ and $\hat{n}$ are both $O(1)$. If we now seek an inner solution to the Helmholtz equation in the form $\phi \sim e^{iks}\hat{A}(\hat{s},\hat{n})$, then the leading order scattered amplitude $\hat{A}$ satisfies the Fock–Leontovič equation [5]

$$\frac{\partial^2 \hat{A}}{\partial \hat{n}^2} + 2i\frac{\partial \hat{A}}{\partial \hat{s}} + 2\hat{n}\hat{A} = 0, \tag{1.3}$$

along with appropriate boundary and far-field conditions. Further details of the derivation of this equation and its solution are given by Babič & Kirpičnikova [6] and Tew *et al.* [7]. These analyses show that the outer limit of the solution in the shadow region close to the surface of the body can be expressed as a sum of exponentially-decaying surface modes, which provide the initial conditions for the creeping surface rays introduced by Keller in the development of the ray approach [1]. As described in Tew *et al.* [7], it is possible to go further and show that there are two transition zones lying either side of the well-known Fresnel region surrounding the shadow boundary. The solutions in these zones provide the matching with the reflected field and the diffracted field radiated by the creeping ray. In these zones, the leading-order amplitudes are functions of $(k/\kappa_0)^{\frac{1}{3}}(y/x)$, where y is the transverse distance from the shadow boundary. All of this analysis assumes that $k \gg \kappa_0$, in which case the width of these transition zones scales with $(k/\kappa_0)^{-\frac{1}{3}}$. However, if $\kappa_0 = O(k)$ then the transition zones merge with the reflected and diffracted fields. We can also see directly from the scalings in (1.2) that the Fock–Leontovič analysis will fail if the curvature and wavenumber are

comparable. This is intuitively clear, since in this limit the curved tip of the object begins to mimic a straight edge and the *exponentially* decaying structure of the creeping ray and associated diffracted field must somehow be replaced by the *algebraically* decaying radial field in (1.1). This cannot be predicted directly from the solution of (1.3).

What we are looking for, then, is the canonical intermediate case of scattering by a 'slender' body for which the inner diffraction structure near the tip satisfies neither the Sommerfeld nor the Fock–Leontovič approximations, but which approaches these solutions as the body becomes sharper or blunter, respectively, exposing the transition between the radial and creeping fields just mentioned. Our main purposes in this paper are to identify the scalings appropriate for such a slender body and then to use them to provide a full asymptotic description of the field that is scattered when the body is subject to plane wave incidence. We will achieve this by the construction of an outer solution which is valid away from the boundary of the body, inner ('tip') solutions, and creeping fields. These various expansions are matched to provide the complete wavefield structure.

There is some existing literature on diffraction by slender bodies. In the outline that follows it is assumed that lengths are scaled to give the Helmholtz equation (2.4) with $k \gg 1$.

In the work which is most closely related to what follows, Mei and Tuck [8] have considered scattering by a two-dimensional slender body (in the context of shallow-water wave theory) in the case of an incoming plane wave at zero angle of incidence. The aspect ratio of the body was taken to be $o(k^{-\frac{1}{2}})$ or $O(k^{-\frac{1}{2}})$. Bigg [9] further analysed this problem by matched asymptotic expansions, taking the aspect ratio to be $O(k^{-\frac{1}{\alpha}})$ with $0 < \alpha \leqslant 2$. The case $\theta_i = 0$ is very special in terms of our analysis, there being no shadow region, and taking the aspect ratio to be $o(k^{-\frac{1}{2}})$, as is for the most part done in these papers, greatly simplifies the analysis of the creeping field.

Most of the literature on diffraction by slender bodies concerns three-dimensional bodies which are slender in two directions. In this case there is again little or no shadow region and the results are of very limited relevance to what follows. Nevertheless, we note the three papers [10, 11, 12] which concern bodies with length (l) being $O(k^{-1})$ and with the diameter of the cross section (d) being $o(k^{-1})$; in [13] and [14] these scalings are replaced by $l \gg k^{-1}$, $d = O(k^{-1})$. In [15] scattering by a curved wire is considered for $l \gg k^{-1}$ and $d \ll k^{-1}$, while [16] also considers the case $d \ll l \ll k^{-1}$; see elsewhere [17, 18] for related results. The paper by Andronov & Bouche [19] is also concerned with strongly prolate bodies, with binormal radius of curvature of $O(k^{-\frac{1}{3}})$ or $O(k^{-\frac{2}{3}})$. With the exception of Andronov & Bouche [19], these papers therefore all assume the thickness of the body to be at most comparable to the wavelength, whereas our analysis primarily concerns bodies which are much thicker. Some features of the problems are similar, however, notably the need for separate discussions of the outer, tip and surface regions.

As we have already noted one of our aims in this paper is to identify and solve a canonical diffraction problem such that the solution to this *single* problem contains *both* the Sommerfeld and Fock–Leontovič structures in the appropriate limits. In doing so, we shall also identify some new features concerning creeping wave propagation in this canonical geometry and also in the classical (Fock–Leontovič) case.

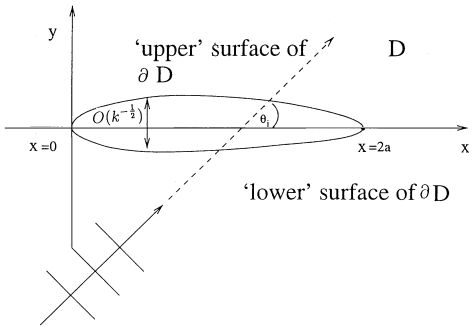

FIGURE 1. A slender body.

2 Formulation of the problem

As we have said, our notion of a 'canonical' slender body is one for which the inner diffraction problem near the point of ray tangency gives the full Helmholtz balance with a nontrivial boundary curve, rather than approximations resulting in either the Sommerfeld or the Fock–Leontovič solution. For this to happen the scalings (1.2) must be replaced by

$$s = k^{-1}\hat{s}, \quad n = k^{-1}\hat{n}, \tag{2.1}$$

and this implies that the local radius of curvature κ_0^{-1} must be $O(k^{-1})$. The width of a closed, convex body away from the tip regions will then generically be $O(k^{-\frac{1}{2}})$, and so we take the lower part of the surface ∂D (see Figure 1) to be of the form

$$y = -k^{-\frac{1}{2}} f(x), \quad (x, y) \in \partial D, \tag{2.2}$$

with, generically,

$$f(x) \sim \beta(2x)^{\frac{1}{2}} \quad \text{as} \quad x \to 0. \tag{2.3}$$

The origin of the coordinate system is located at the left-hand tip, and the $O(1)$ constant β is the curvature of ∂D at the origin. The function $f(x)$ is taken to be independent of k. The problem can now be posed as determining the asymptotic solution as $k \to \infty$ of the Helmholtz equation

$$(\nabla^2 + k^2)\phi = 0 \tag{2.4}$$

in the region D exterior to ∂D subject to the boundary condition

$$\frac{\partial \phi}{\partial n} = 0 \tag{2.5}$$

on ∂D. We also require that $\phi - \mathrm{e}^{ik(x\cos\theta_i + y\sin\theta_i)}$ be both outgoing and diminishing in amplitude as $(x^2 + y^2)^{\frac{1}{2}} \to \infty$. Note that a time-harmonic factor $\mathrm{e}^{-i\omega t}$ (with $k = \omega/c$) has been assumed, and that $e^{ik(x\cos\theta_i + y\sin\theta_i)}$ represents the incident plane wave.

The large k assumption allows the incoming wave to be represented by a family of parallel rays. Those that are incident upon ∂D will yield a reflected ray field. Of course, this will not occur at all points on ∂D and the remaining portion lies within the shadow zone whose outer edges are defined by the limiting incident rays impinging upon the 'tips' of the body. All other incoming rays miss the obstacle altogether and propagate unimpeded. These simple observations illustrate the need for three different descriptions

https://doi.org/10.1017/S0956792598003441 Published online by Cambridge University Press

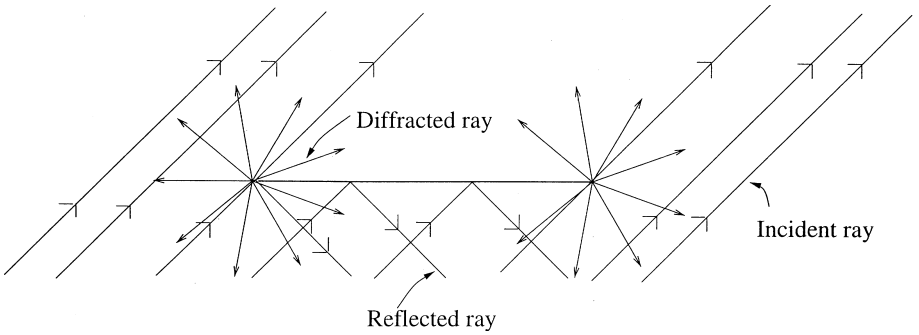

FIGURE 2. The 'outer' ray picture.

of the solution, depending on the region under consideration: (i) a 'geometrical optics' description away from the body, (ii) a creeping wavefield on and close to the surface of the body, but away from its ends and (iii) an inner problem for each tip which involves solving the full Helmholtz equation for plane wave incidence upon a parabolic boundary; this solution, when matched to (i), will provide the directivity coefficients which cannot be calculated from the outer analysis.

We shall first calculate the geometrical optics contribution and then follow this with a thorough examination of the inner problem to find the required diffraction coefficients. We shall study the problem for all values of the angle of incidence θ_i in the range $0 \leqslant \theta_i \leqslant \pi$; the cases with $-\pi < \theta_i < 0$ follow immediately by reflection about the x axis. We then describe the creeping fields, which have a number of novel features, and we conclude with some discussion. Results for the special case in which the body is an ellipse are summarised in Appendix A. Appendix B contains a list of results for parabolic cylinder functions used in the paper.

3 Outer 'ray' field

To determine the outer (ray) solution, we first consider the reflection of rays incident upon the lower section of the boundary at points other than the two tips. The regions in which the various ray fields exist are indicated in Figure 2. We begin by writing

$$\phi(x, y) = \mathrm{e}^{ik(x\cos\theta_i + y\sin\theta_i)} + A_0(x, y)\mathrm{e}^{iku(x,y) + ik^{\frac{1}{2}}U(x,y)} + O(k^{-\frac{1}{2}}), \tag{3.1}$$

where A_0 is the leading order amplitude of the 'outer' scattered field and the two functions u and U are to be determined. This ansatz is motivated by the fact that on this part of the boundary ∂D, given by (2.2), the incident field is $\exp(ikx\cos\theta_i - ik^{\frac{1}{2}}f(x)\sin\theta_i)$.

Substituting (3.1) into the Helmholtz equation (2.4) and extracting like powers of k leads to

$$\nabla u \cdot \nabla u = 1, \tag{3.2}$$

$$\nabla u \cdot \nabla U = 0, \tag{3.3}$$

and

$$A_0\nabla^2 u + 2\nabla A_0 \cdot \nabla u + iA_0\nabla U \cdot \nabla U = 0. \tag{3.4}$$

https://doi.org/10.1017/S0956792598003441 Published online by Cambridge University Press

The boundary condition for u follows from (3.1) as

$$u(x,0) = x\cos\theta_i, \tag{3.5}$$

so by (3.2)

$$u(x,y) = x\cos\theta_i - y\sin\theta_i. \tag{3.6}$$

Equations (3.6) and (3.3) imply that

$$U(x,y) = -2\sin\theta_i f(x + y\cot\theta_i), \tag{3.7}$$

where we have imposed the associated boundary condition

$$U(x,0) = -2\sin\theta_i f(x), \tag{3.8}$$

which follows from (3.1) because

$$u(x, -k^{-\frac{1}{2}}f(x)) = x\cos\theta_i - k^{-\frac{1}{2}}f(x)\sin\theta_i. \tag{3.9}$$

Similarly, the boundary condition on A_0 turns out to be

$$A_0(x,0) = \mathrm{e}^{2if(x)f'(x)}. \tag{3.10}$$

Solving (3.4) subject to (3.10), we find that

$$A_0(x,y) = \exp\left[\frac{2iy}{\sin\theta_i}(f'(x + y\cot\theta_i))^2 - 2i\cos\theta_i f(x + y\cot\theta_i)f'(x + y\cot\theta_i)\right], \tag{3.11}$$

from which the leading order reflected field propagating into $y < 0$ now follows.

In addition to the incident and reflected fields, the outer solution also contains two diffracted fields, the tips each giving rise to an expansion fan of scattered rays (see Figure 2). This leads to a diffracted field of the form

$$\phi^{(d)} \sim \frac{F(\theta)\mathrm{e}^{ikr}}{\sqrt{kr}} \quad \text{as} \quad k \to \infty \quad \text{with} \quad r = O(1) \tag{3.12}$$

from the left-hand tip, with a similar result holding for the other. The crucial point to note here is that the tip is locally parabolic and so the directivity function $F(\theta)$ is not in general given by (1.1). We must therefore examine the inner problem in order to determine this aspect of the outer solution.

4 Inner diffraction analysis

4.1 Background

The diffraction of a plane wave by a parabolic cylinder (see Figure 3) has been considered many times before (see, for example, [20–27]), though one significant difference between our analysis and much of the other literature is that the wavenumber k scales out of our problem; elsewhere it is often taken to be a large asymptotic parameter.

One way of posing and solving this problem is to decompose the incoming plane wave into an infinite sum of appropriate parabolic cylinder functions and then add to this another such sum so that the radiation and boundary conditions are simultaneously satisfied. Ivanov [20] took this approach for the restricted range of angles of incidence θ_i in the region $-\frac{\pi}{2} < \theta_i < \frac{\pi}{2}$. Though this works well for low frequencies, the resulting sum is slow to converge for large values of k. One way of overcoming this problem is

https://doi.org/10.1017/S0956792598003441 Published online by Cambridge University Press

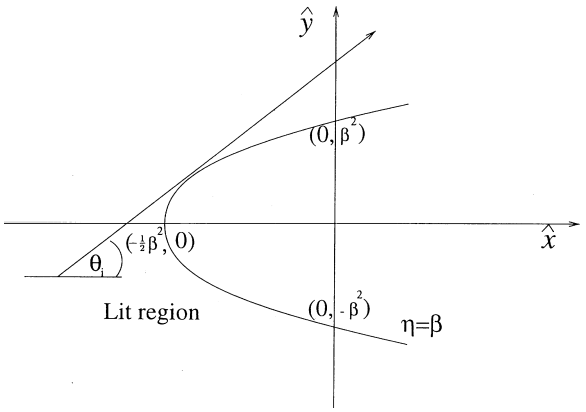

FIGURE 3. The inner parabolic tip structure.

to convert the sum into an integral using a Watson transform [28] and then to analyse the integral using standard asymptotic techniques in the limit $k \to \infty$, and Ivanov [20] goes on to use this procedure. Rice [22] also adopted this methodology, and states that the resultant integral is valid for the full-range required, $0 < \theta_i < \pi$. The residue sum solution that results contains, for $0 < \theta_i < \frac{\pi}{2}$, parabolic cylinder functions of integer order, whereas for $\frac{\pi}{2} < \theta_i < \pi$ they are of non-integer order; for $\theta_i = \frac{\pi}{2}$ which sum is valid is dependent on (x, y). Another approach (see Jones [24] and Ott [25]) uses a representation, due to Cherry [29], for the incident plane wave in terms of integrated parabolic cylinder functions; it can easily be shown that the resulting integral solution is equivalent to that obtained by Ivanov. Hochstadt [23] uses a Green's function representation, the scattered field being given by a multiple integral which is evaluated in the high frequency limit. The more direct way of analysing the limit as $k \to \infty$ by using the geometrical theory of diffraction has been implemented by Keller [26]. The special case $\theta_i = 0$, for which the incident field propagates parallel to the axis of the cylinder, can be solved in closed form in terms of a Fresnel integral (Lamb [27]), and this case has also been studied asymptotically for $k \to \infty$ using geometrical optics (Keller *et al.* [30]).

As already noted, we are not here concerned with the limit $k \to \infty$; instead we need to determine the far-field behaviour for $k = 1$, and this will also rely on having an integral representation of the solution. We introduce an inner coordinate system $(\hat{x}, \hat{y})$ defined by

$$x = k^{-1}\left(\hat{x} + \frac{\beta^2}{2}\right), \quad y = k^{-1}\hat{y} \tag{4.1}$$

and the parabolic cylinder coordinates (ξ, η) given by

$$\hat{x} = \frac{\xi^2 - \eta^2}{2}, \qquad \hat{y} = \eta\xi, \tag{4.2}$$

where $\xi \in (-\infty, \infty), \eta \in (0, \infty)$ and the parabola is given by $\eta = \beta$. In these inner coordinates (from which the hats will be dropped for the rest of this section) the leading order inner problem for the total potential is

$$\frac{\partial^2\phi}{\partial\xi^2} + \frac{\partial^2\phi}{\partial\eta^2} + (\xi^2 + \eta^2)\phi = 0, \quad \eta > \beta, \tag{4.3}$$

https://doi.org/10.1017/S0956792598003441 Published online by Cambridge University Press

$$\frac{\partial \phi}{\partial \eta} = 0, \quad \eta = \beta. \tag{4.4}$$

In the far-field we require that $\phi - \mathrm{e}^{i(x\cos\theta_i + y\sin\theta_i)}\mathrm{e}^{\frac{i\beta^2}{2}\cos\theta_i}$ satisfy an outgoing wave condition, where the term subtracted from ϕ is the incident field in its inner form.

4.2 Solution to the Sommerfeld diffraction problem

We first note the solution to the classical Sommerfeld half-plane diffraction problem, being the solution to (4.3) and (4.4) with $\beta = 0$. We denote this Sommerfeld solution by ϕ_s, which can be written in the following equivalent forms, all valid for $0 < \theta < 2\pi$:

$$\phi_s = \frac{\mathrm{e}^{-\frac{i\pi}{4}}}{\sqrt{\pi}}\left[-\mathrm{e}^{ir\cos(\theta-\theta_i)}F\left(\sqrt{2r}\sin\frac{\theta-\theta_i}{2}\right) + \mathrm{e}^{ir\cos(\theta+\theta_i)}F\left(\sqrt{2r}\sin\frac{\theta+\theta_i}{2}\right)\right], \quad 0 < \theta_i < \pi \tag{4.5}$$

$$= \frac{\mathrm{e}^{-\frac{i\pi}{4}}}{\sqrt{\pi}}\mathrm{e}^{-ir\cos\theta}F\left(\sqrt{2r}\cos\frac{\theta}{2}\right), \quad \theta_i = \pi \tag{4.6}$$

$$= \frac{i}{2\sqrt{2\pi}}\int_{-\frac{1}{2}-i\infty}^{-\frac{1}{2}+i\infty}\frac{\left(\tan\frac{\theta_i}{2}\right)^{\nu}}{\cos\frac{\theta_i}{2}}\left[D_{-1-\nu}(-\bar{p}\eta) + D_{-1-\nu}(\bar{p}\eta)\right]D_{\nu}(\bar{p}\xi)\frac{d\nu}{\sin\nu\pi}, \quad 0 < \theta_i < \pi \tag{4.7}$$

$$= \frac{1}{\sqrt{2\pi}\cos\frac{\theta_i}{2}}\sum_{n=0}^{\infty}\left(-\tan\frac{\theta_i}{2}\right)^{n}\left[D_{-1-n}(-\bar{p}\eta) + D_{-1-n}(\bar{p}\eta)\right]D_n(\bar{p}\xi), \quad 0 < \theta_i < \frac{\pi}{2} \tag{4.8}$$

$$= \frac{\sqrt{2}}{\sqrt{\pi}\cos\frac{\theta_i}{2}}\sum_{n=0}^{\infty}\left(\tan\frac{\theta_i}{2}\right)^{-1-2n}D_{2n}(\bar{p}\eta)D_{-1-2n}(\bar{p}\xi), \quad \frac{\pi}{2} < \theta_i < \pi \tag{4.9}$$

$$= \frac{1}{\sqrt{2\pi}}D_{-1}(\bar{p}\xi)D_0(\bar{p}\eta), \quad \theta_i = \pi. \tag{4.10}$$

In the case $\theta_i = \pi$ the incident plane wave is taken to lie in $y < 0$; if it exists in $y > 0$ instead then ξ is replaced in (4.10) by $-\xi$ and $\sqrt{2r}\cos\frac{\theta}{2}$ is replaced in (4.6) by $-\sqrt{2r}\cos\frac{\theta}{2}$. When $\theta_i = \pi/2$ then (4.8) is valid for $\xi < \eta$ and (4.9) for $\xi > \eta$. In these expressions $p = \sqrt{2i}$, $\bar{p} = \sqrt{-2i}$, the D_ν are parabolic cylinder functions (as defined in [31, 32]) and F is the Fresnel integral defined by Bowman *et al.* [4] as

$$F(x) = \int_x^{\infty}\mathrm{e}^{it^2}\mathrm{d}t = \frac{\sqrt{\pi}}{2}\mathrm{e}^{\frac{i\pi}{4}}\mathrm{erfc}(\mathrm{e}^{-\frac{i\pi}{4}}x). \tag{4.11}$$

The far-field asymptotics of ϕ_s are easily derived from (4.5), giving as $r \to \infty$

$$\phi_s \sim \mathrm{e}^{ir+\frac{i\pi}{4}}\left(\frac{2}{r\pi}\right)^{\frac{1}{2}}\frac{\cos\frac{\theta}{2}\sin\frac{\theta_i}{2}}{(\cos\theta - \cos\theta_i)}, 0 < \theta < \theta_i, \tag{4.12}$$

$$\sim \mathrm{e}^{ir\cos(\theta-\theta_i)} + \mathrm{e}^{ir+\frac{i\pi}{4}}\left(\frac{2}{r\pi}\right)^{\frac{1}{2}}\frac{\cos\frac{\theta}{2}\sin\frac{\theta_i}{2}}{(\cos\theta - \cos\theta_i)}, \theta_i < \theta < 2\pi - \theta_i, \tag{4.13}$$

$$\sim \mathrm{e}^{ir\cos(\theta-\theta_i)} + \mathrm{e}^{ir\cos(\theta+\theta_i)} + e^{ir+\frac{i\pi}{4}}\left(\frac{2}{r\pi}\right)^{\frac{1}{2}}\frac{\cos\frac{\theta}{2}\sin\frac{\theta_i}{2}}{(\cos\theta - \cos\theta_i)}, \quad 2\pi - \theta_i < \theta < 2\pi. \tag{4.14}$$

https://doi.org/10.1017/S0956792598003441 Published online by Cambridge University Press

Equation (4.12) represents a diffracted field, (4.13) incident and diffracted fields and (4.14) incident, reflected and diffracted fields. These expressions are not valid for $\theta = \theta_i$ and $\theta_i = 2\pi - \theta$, which are, respectively, the shadow boundaries for the incident and reflected fields.

4.3 Exact solution to the full diffraction problem

4.3.1 *Integral representations*

An exact solution of the problem for the total potential defined by Eqs. (4.3) and (4.4) can be written down in terms of integrated parabolic cylinder functions [4, 24] in the form

$$\phi = \frac{ie^{i\frac{\beta^2}{2}\cos\theta_i}}{2\sqrt{2\pi}} \int_{-\frac{1}{2}-i\infty}^{-\frac{1}{2}+i\infty} \frac{\left(\tan\frac{\theta_i}{2}\right)^{\nu}}{\cos\frac{\theta_i}{2}} \left[D_{-1-\nu}(-\bar{p}\eta) + \frac{D'_{-1-\nu}(-\bar{p}\beta)}{D'_{-1-\nu}(\bar{p}\beta)} D_{-1-\nu}(\bar{p}\eta)\right] D_{\nu}(\bar{p}\xi) \frac{d\nu}{\sin\nu\pi}. \tag{4.15}$$

This solution is valid for $0 < \theta_i < \pi$ though, as we shall see, some aspects of its evaluation are dependent upon whether or not $\theta_i < \frac{\pi}{2}$. To avoid carrying the factor $\exp(i\beta^2\cos\theta_i/2)$ in the analysis that follows, we work in terms of the potential Φ defined by $\phi = \Phi\exp(i\beta^2\cos\theta_i/2)$.

Since

$$D_{-\nu-1}(-\bar{p}\eta) + \frac{D'_{-1-\nu}(-\bar{p}\beta)}{D'_{-1-\nu}(\bar{p}\beta)} D_{-1-\nu}(\bar{p}\eta) = \frac{\sqrt{2\pi}}{\Gamma(\nu+1)}(-i)^{\nu}\left[D_{\nu}(p\eta) - \frac{iD'_{\nu}(p\beta)}{D'_{-1-\nu}(\bar{p}\beta)} D_{-\nu-1}(\bar{p}\eta)\right], \tag{4.16}$$

this integral solution can also be expressed as

$$\Phi = \frac{i}{2\cos\frac{\theta_i}{2}} \int_{-\frac{1}{2}-i\infty}^{-\frac{1}{2}+i\infty} \frac{\left(-i\tan\frac{\theta_i}{2}\right)^{\nu}}{\Gamma(\nu+1)} \left[D_{\nu}(p\eta) - \frac{iD'_{\nu}(p\beta)}{D'_{-1-\nu}(\bar{p}\beta)} D_{-1-\nu}(\bar{p}\eta)\right] D_{\nu}(\bar{p}\xi) \frac{d\nu}{\sin\nu\pi}. \tag{4.17}$$

This is the expression derived by Ivanov [20], though there it was implicitly assumed that the range of angles of incidence is restricted to $0 < \theta_i < \frac{\pi}{2}$. The first term in the integrand in (4.17) is an integral representation of the incident plane wave and an equivalent series representation is

$$e^{ik(x\cos\theta_i + y\sin\theta_i)} = \sec\frac{\theta_i}{2} \sum_{n=0}^{\infty} \frac{\left(i\tan\frac{\theta_i}{2}\right)^n}{n!} D_n(\bar{p}\zeta) D_n(p\eta), \quad -\frac{\pi}{2} < \theta_i < \frac{\pi}{2}. \tag{4.18}$$

4.3.2 *Series representations*

It is possible to re-express the integral solution in terms of an exact residue series, a procedure which depends upon the sign of $\theta_i - \frac{\pi}{2}$. If $0 < \theta_i < \frac{\pi}{2}$ we can complete the original path of integration, in (4.15), using an arc at infinity in the right-hand half plane in which case the simple poles that contribute are the zeros of $\sin(\nu\pi)$. This leads to the

https://doi.org/10.1017/S0956792598003441 Published online by Cambridge University Press

equivalent exact representations

$$\Phi = \frac{1}{\sqrt{2\pi}\cos\frac{\theta_i}{2}} \sum_{n=0}^{\infty} \left(-\tan\frac{\theta_i}{2}\right)^n [D_{-1-n}(-\bar{p}\eta) + \frac{D'_{-1-n}(-\bar{p}\beta)}{D'_{-1-n}(\bar{p}\beta)} D_{-1-n}(\bar{p}\eta)] D_n(\bar{p}\xi) \quad (4.19)$$

$$= \frac{e^{ix}}{2\cos\frac{\theta_i}{2}} \sum_{n=0}^{\infty} \left(-\tan\frac{\theta_i}{2}\right)^n H_n(e^{-\frac{i\pi}{4}}\xi) \left[i^n \mathrm{erfc}(-e^{-\frac{i\pi}{4}}\eta) \right. \quad (4.20)$$

$$\left. + \frac{2(n+1)i^n\mathrm{erfc}(-e^{-\frac{i\pi}{4}}\beta) - e^{-\frac{i\pi}{4}}\beta i^{n+1}\mathrm{erfc}(-e^{-\frac{i\pi}{4}}\beta)}{2(n+1)i^n\mathrm{erfc}(e^{-\frac{i\pi}{4}}\beta) + e^{-\frac{i\pi}{4}}\beta i^{n+1}\mathrm{erfc}(e^{-\frac{i\pi}{4}}\beta)} i^n\mathrm{erfc}(e^{-\frac{i\pi}{4}}\eta) \right], \quad (4.21)$$

where H_n is the Hermite polynomial of degree n and i^n is the integral operator defined in [33] as

$$i^n\mathrm{erfc}(z) = \int_z^{\infty} i^{n-1}\mathrm{erfc}(t)\mathrm{d}t, \quad (n = 0, 1, 2, \ldots), \quad (4.22)$$

and

$$i^{-1}\mathrm{erfc}(z) = \frac{2}{\sqrt{\pi}} e^{-z^2}, \quad i^0\mathrm{erfc}(z) = \mathrm{erfc}(z). \quad (4.23)$$

If $\frac{\pi}{2} < \theta_i < \pi$, then the analogous expression is

$$\Phi = \frac{-\sqrt{\pi}}{\sqrt{2}\cos\frac{\theta_i}{2}} \sum_{n=0}^{\infty} \frac{\left(\tan\frac{\theta_i}{2}\right)^{\nu_n}}{\sin \nu_n\pi} D_{\nu_n}(\bar{p}\xi) D_{-1-\nu_n}(\bar{p}\eta) \frac{D'_{-1-\nu_n}(-\bar{p}\beta)}{\frac{\partial}{\partial\nu} D'_{-1-\nu}(\bar{p}\beta)|_{\nu=\nu_n}}. \quad (4.24)$$

The difference in structure in these two ranges of θ_i arises because in the second case we must complete the contour in the left half-plane, capturing residue contributions from the simple poles at $\nu = \nu_n$, where the ν_n are the solutions of the transcendental equation

$$D'_{-1-\nu}(\bar{p}\beta) = 0. \quad (4.25)$$

These roots all have $\mathrm{Re}(\nu) \leqslant -1$, $\mathrm{Im}(\nu) \leqslant 0$. The different forms of the ξ and η dependence of (4.19) and (4.24) can also be derived by elementary separation of variables considerations, but the calculation of the corresponding coefficients is non-trivial.

If $\theta_i = \frac{\pi}{2}$ then which way the path of integration is completed is dependent on ξ, η: for $\xi < \eta$ then Eq. (4.19) is valid and for $\xi > \eta$ (4.24) holds.

4.4 Far-field behaviour

4.4.1 $\beta = O(1)$

Having derived exact representations for the total potential in several distinct forms, we now examine the corresponding far-field structure. To do so, it is easier to use the integral (rather than the series) representations, since standard residue and stationary phase methods can be applied directly.

The far-field structure depends on the polar angle θ. In particular, we anticipate a different asymptotic form in the geometrical shadow from that in the illuminated zone. This manifests itself in the way that we evaluate the integrals asymptotically, since the

https://doi.org/10.1017/S0956792598003441 Published online by Cambridge University Press

particular range of θ dictates which way complex integration paths are closed to trap the appropriate residue contributions.

It turns out that there are three distinct ranges of θ (which, like r below, is now measured from the origin of the displaced inner coordinates defined at the end of §4.1) which necessitate separate analyses. These are $2\pi - \theta_i < \theta < 2\pi$, $\theta_i < \theta < 2\pi - \theta_i$ and $0 < \theta < \theta_i$. For the classical Sommerfeld problem, these correspond to the fully illuminated ($\equiv$ incident, reflected and diffracted fields), illuminated ($\equiv$ incident and diffracted fields) and geometrical shadow ($\equiv$ diffracted field) zones, respectively. However, for bodies of $O(1)$ aspect ratio (corresponding to $\beta \to \infty$) the shadow boundaries of the incident and reflected fields coincide (at $\theta = \theta_i$); we return to this distinction shortly.

(a) $2\pi - \theta_i < \theta < 2\pi$

Whichever integral representation we use, we must apply the connection formula (B 3) to the $D_v(\bar{p}\xi)$ term because, in this range, ξ is large in magnitude and negative and so the argument of this parabolic cylinder function lies exactly on an anti-Stokes line. This gives the solution for Φ in the form

$$\begin{aligned}\Phi = {} & \frac{i}{2\sqrt{2\pi}} \int_{-\frac{1}{2}-i\infty}^{-\frac{1}{2}+i\infty} \frac{(\tan\frac{1}{2}\theta_i)^v}{\cos\frac{1}{2}\theta_i} D_{-1-v}(-\bar{p}\eta) D_v(\bar{p}\xi) \frac{dv}{\sin(v\pi)} \\ & + \frac{i}{2\sqrt{2\pi}} \int_{-\frac{1}{2}-i\infty}^{-\frac{1}{2}+i\infty} \frac{(\tan\frac{1}{2}\theta_i)^v}{\cos\frac{1}{2}\theta_i} \mathrm{e}^{v\pi i} \frac{D'_{-1-v}(-\bar{p}\beta)}{D'_{-1-v}(\bar{p}\beta)} D_{-1-v}(\bar{p}\eta) D_v(-\bar{p}\xi) \frac{dv}{\sin(v\pi)} \\ & + \frac{1}{2\pi} \int_{-\frac{1}{2}-i\infty}^{-\frac{1}{2}+i\infty} \frac{(\tan\frac{1}{2}\theta_i)^v}{\cos\frac{1}{2}\theta_i} \frac{D'_{-1-v}(-\bar{p}\beta)}{D'_{-1-v}(\bar{p}\beta)} \mathrm{e}^{\frac{v\pi i}{2}} \Gamma(1+v) D_{-1-v}(\bar{p}\eta) D_{-1-v}(-i\bar{p}\xi) dv. \end{aligned} \tag{4.26}$$

We must estimate each of these integrals asymptotically as $\xi \to -\infty, \eta \to \infty$ for $\beta = O(1)$. The first integral can be evaluated explicitly in terms of a complementary error function and is actually one of the terms in the Sommerfeld solution (4.5) (cf. (4.7)). For the second integral, we replace the ξ and η-dependent parabolic cylinder functions by the leading term in their asymptotic expansions and evaluate the resulting integral exactly by completing the path of integration with an arc at infinity in the left-half plane. Two sets of residues contribute: the negative integers (for which $\sin(v\pi) = 0$) and the roots of (4.25). The third integral necessitates replacing the parabolic cylinder functions for large $|\xi|$ and η by their Darwin expansions and then performing a stationary phase analysis. The upshot is that this integral supplies the reflected field.

Collecting these results together, the far-field response is found in the form

$$\begin{aligned}\Phi \sim {} & \mathrm{e}^{i(x\cos\theta_i + y\sin\theta_i)} \\ & + \exp\Big[i(x\cos\theta_i - y\sin\theta_i) - 2^{\frac{3}{2}}\beta i \sin^{\frac{1}{2}}\theta_i (x\sin\theta_i + y\cos\theta_i)^{\frac{1}{2}} \\ & - i\beta^2 \sin\theta_i \left(\frac{x\cos\theta_i - y\sin\theta_i}{x\sin\theta_i + y\cos\theta_i} \right) - i\beta^2\cos\theta_i \Big] \\ & - \sqrt{\frac{\pi}{2r}} \frac{\mathrm{e}^{ir + \frac{i\pi}{4}}}{2\cos\frac{1}{2}\theta_i \sin\frac{1}{2}\theta} \sum_{n=0}^{\infty} \left(\frac{\tan\frac{1}{2}\theta_i}{|\tan\frac{1}{2}\theta|} \right)^{v_n} \frac{e^{v_n\pi i}}{\sin(v_n\pi)} \frac{D'_{-1-v_n}(-\bar{p}\beta)}{\frac{\partial}{\partial v} D'_{-1-v}(\bar{p}\beta)|_{v=v_n}}, \end{aligned} \tag{4.27}$$

https://doi.org/10.1017/S0956792598003441 Published online by Cambridge University Press

where the v_n are defined in (4.25). There is an $O(r^{-\frac{1}{2}})$ term omitted from the second term in (4.27), which comes from the next order term in the stationary phase calculation. However, this has the same phase as (and should be regarded as part of) the reflected field and does not contribute to the diffracted field. We emphasize that (4.27) is written in terms of the inner variables with hats omitted.

In (4.27), the first term on the right-hand side is the incident field and the second is the reflected field. The latter should match the result derived in §3 once it has been expressed in terms of the outer coordinates. In the limit considered here, we can take $f(x) \sim 2(\beta x)^{\frac{1}{2}}$ in that calculation and it is then straightforward to see that there is indeed a perfect match. The final term in Eq. (4.27) is the diffracted field.

(b) $\theta_i < \theta < 2\pi - \theta_i$

In this region ξ changes sign and the cases $\xi < 0$ and $\xi > 0$ must be treated separately. In the former case, we use the representation (4.26), except that now the evaluation of the second integral involves completing the path of integration to the right and only the simple poles at the non-negative integers contribute. The stationary phase estimate resulting from the third integral is now exponentially small and is therefore ignored; it may be interpreted as complex ray reflection from the analytical continuation of the boundary, cf. [34].

For $\xi > 0$, we no longer need to use the connection formula on $D_v(\bar{p}\xi)$ and the leading-order scattered potential is found to be

$$\Phi \sim \mathrm{e}^{i(x\cos\theta_i + y\sin\theta_i)} + \frac{\mathrm{e}^{ir-\frac{i\pi}{4}}}{2\sqrt{r}\cos\frac{1}{2}\theta_i \sin\frac{1}{2}\theta} \sum_{n=0}^{\infty} \frac{1}{n!} \left(\frac{i\tan\frac{1}{2}\theta_i}{\tan\frac{1}{2}\theta} \right)^n \frac{D_n'(p\beta)}{D_n'(\bar{p}\beta)}, \tag{4.28}$$

regardless of the sign of ξ.

(c) $0 < \theta < \theta_i$

This is the geometrical shadow and is treated by recombining the second and third terms in (4.26) using the connection formula in reverse and then enclosing the integral to the left, having first replaced the parabolic cylinder functions by the first terms in their normal asymptotic expansions. The field is purely diffracted and has the series representation

$$\Phi \sim -\frac{\mathrm{e}^{ir+\frac{i\pi}{4}}}{2\cos\frac{1}{2}\theta_i \sin\frac{1}{2}\theta} \sqrt{\frac{\pi}{2r}} \sum_{n=0}^{\infty} \left(\frac{\tan\frac{1}{2}\theta_i}{\tan\frac{1}{2}\theta} \right)^{\nu_n} \frac{D'_{-1-\nu_n}(-\bar{p}\beta)}{\frac{\partial}{\partial\nu} D'_{-1-\nu}(\bar{p}\beta)|_{\nu=\nu_n}} \frac{1}{\sin(\nu_n\pi)}. \tag{4.29}$$

The directivity $F(\theta)$ in §3 can now be read off from (4.27), (4.28) and (4.29). We note that the angles θ based on the inner and outer coordinate systems are asymptotically equivalent when performing this matching; this is not true of the r variables, leading to an extra factor $\exp(-i\beta^2\cos\theta/2)$ when matching. This highlights a need for care when defining directivity functions – a shift of the source location of a cylindrically spreading wavefield by an $O(k^{-1})$ amount induces an $O(1)$ change in the directivity. Remembering

https://doi.org/10.1017/S0956792598003441 Published online by Cambridge University Press

to also reinstate the $\exp(i\beta^2\cos\theta_i/2)$ prefactor to obtain ϕ from Φ, we have

$$F(\theta) = -\sqrt{\frac{\pi}{2}}\frac{\mathrm{e}^{\frac{i\pi}{4}}\mathrm{e}^{\frac{i\beta^2}{2}(\cos\theta_i-\cos\theta)}}{2\cos\tfrac{1}{2}\theta_i\sin\tfrac{1}{2}\theta}\sum_{n=0}^{\infty}\left(\frac{\tan\frac{1}{2}\theta_i}{|\tan\frac{1}{2}\theta|}\right)^{\nu_n}\frac{\mathrm{e}^{\nu_n\pi i}D'_{-1-\nu_n}(-\bar{p}\beta)}{\sin(\nu_n\pi)\frac{\partial}{\partial\nu}D'_{-1-\nu}(\bar{p}\beta)|_{\nu=\nu_n}},$$
$$2\pi-\theta_i<\theta<2\pi, \tag{4.30}$$

$$=\frac{\mathrm{e}^{-\frac{i\pi}{4}}\mathrm{e}^{i\frac{\beta^2}{2}(\cos\theta_i-\cos\theta)}}{2\cos\tfrac{1}{2}\theta_i\sin\tfrac{1}{2}\theta}\sum_{n=0}^{\infty}\frac{1}{n!}\left(\frac{i\tan\frac{1}{2}\theta_i}{\tan\frac{1}{2}\theta}\right)^{n}\frac{D'_n(p\beta)}{D'_n(\bar{p}\beta)},\quad \theta_i<\theta<2\pi-\theta_i, \tag{4.31}$$

$$=-\frac{\mathrm{e}^{\frac{i\pi}{4}}\mathrm{e}^{i\frac{\beta^2}{2}(\cos\theta_i-\cos\theta)}}{2\cos\tfrac{1}{2}\theta_i\sin\tfrac{1}{2}\theta}\sqrt{\frac{\pi}{2}}\sum_{n=0}^{\infty}\left(\frac{\tan\frac{1}{2}\theta_i}{\tan\frac{1}{2}\theta}\right)^{\nu_n}\frac{D'_{-1-\nu_n}(-\bar{p}\beta)}{\sin(\nu_n\pi)\frac{\partial}{\partial\nu}D'_{-1-\nu}(\bar{p}\beta)|_{\nu=\nu_n}},$$
$$0<\theta<\theta_i. \tag{4.32}$$

We have thus now established series representations for the directivity function $F(\theta)$ and have demonstrated that it has different analytical structure depending upon the region in which we are evaluating it. It can also be represented by the unified expression

$$F(\theta)=\frac{\mathrm{e}^{\frac{i\pi}{4}}\mathrm{e}^{i\frac{\beta^2}{2}(\cos\theta_i-\cos\theta)}}{2\sqrt{2\pi}\sin\frac{1}{2}(\theta_i-\theta)}+\frac{\mathrm{e}^{\frac{3\pi i}{4}}\mathrm{e}^{i\frac{\beta^2}{2}(\cos\theta_i-\cos\theta)}}{4\sqrt{2\pi}\cos\tfrac{1}{2}\theta_i\sin\tfrac{1}{2}\theta}\int_{-\frac{1}{2}-i\infty}^{-\frac{1}{2}+i\infty}\left(\frac{\tan\frac{1}{2}\theta_i}{\tan\frac{1}{2}\theta}\right)^{\nu}\frac{D'_{-1-\nu}(-\bar{p}\beta)}{D'_{-1-\nu}(\bar{p}\beta)}\frac{d\nu}{\sin(\nu\pi)} \tag{4.33}$$

provided we take $(\cot\frac{1}{2}\theta)^{\nu}=|\cot\frac{1}{2}\theta|^{\nu}\mathrm{e}^{\nu\pi i}$ if $\cot\frac{1}{2}\theta<0$. This expression provides a useful integral representation of the directivity to complement the series forms given above.

One of the purposes of this analysis is to understand the transition between the Fock-Leontovič ($\beta\to\infty$) and Sommerfeld ($\beta\to 0$) limits. We now consider these limits, which also act as a useful check on the results we have obtained so far.

4.4.2 *The limit $\beta\to\infty$*

We begin our analysis of the far-field for the large β case by considering the shadow zone, in which the field is given by the single expression in (4.29). In this limit, we are able to estimate the roots ν_n of (4.25) and use them to evaluate the terms in the summand of (4.29). In fact, using the Airy-type expansions that are listed in Appendix B we are able to show that if we set $\nu_n=-\frac{1}{2}+i\mu_n$, where μ_n is complex, then

$$\mu_n=\frac{\beta^2}{2}-\frac{\gamma_n^2\mathrm{e}^{-\frac{2\pi i}{3}}\beta^{\frac{2}{3}}}{2^{\frac{1}{3}}}+O(\beta^{-\frac{1}{3}}) \tag{4.34}$$

as $\beta\to\infty$, where Ai is the standard Airy function and $\mathrm{Ai}'(-\gamma_n^2)=0$. We can then use this result, along with repeated use of the listed uniform expansions, to establish that

$$\frac{D'_{-1-\nu_n}(-\bar{p}\beta)}{\frac{\partial}{\partial\nu}D'_{-1-\nu}(\bar{p}\beta)|_{\nu=\nu_n}}\sim-\frac{\beta^{\frac{2}{3}}\mathrm{e}^{\mu_n\pi}\mathrm{Ai}'(-\gamma_n^2\mathrm{e}^{-\frac{2\pi i}{3}})}{2^{\frac{1}{3}}\gamma_n^2\mathrm{Ai}(-\gamma_n^2)} \tag{4.35}$$

from which the limiting form for Φ, given by

$$\Phi\sim-e^{ir+\frac{i\pi}{4}}\sqrt{\frac{\pi}{r\sin\theta\sin\theta_i}}2^{\frac{1}{6}}\beta^{\frac{2}{3}}\sum_{n=0}^{\infty}\frac{\mathrm{Ai}(-\gamma_n^2\mathrm{e}^{-\frac{2\pi i}{3}})}{\gamma_n^2\mathrm{Ai}(-\gamma_n^2)}\mathrm{e}^{i\mu_n\ln\left(\frac{\tan\frac{1}{2}\theta_i}{\tan\frac{1}{2}\theta}\right)}, \tag{4.36}$$

https://doi.org/10.1017/S0956792598003441 Published online by Cambridge University Press

is immediate. This is then the far-field behaviour of the inner solution in the limit $\beta \to \infty$.

To interpret this solution, we observe that if we scale $\mathbf{x} = \beta^2 \hat{\mathbf{X}}$, then the inner diffraction problem is to solve

$$(\nabla^2 + \beta^4)\phi = 0 \tag{4.37}$$

(where the Laplacian is with respect to $\hat{X}$ and $\hat{Y}$) exterior to the parabola $\hat{Y}^2 = 2\hat{X} + 1$ and subject to

$$\frac{\partial \phi}{\partial \hat{N}} = 0 \tag{4.38}$$

on it, with appropriate conditions at infinity. This is a ray problem (with β^2 replacing the wavenumber k) and so we expect a creeping field to be initiated at the point of tangency between the incoming ray field and the boundary. In this neighbourhood, the solution to the analogue of (1.2)–(1.3) yields a modal expansion for this limit of the creeping field that propagates into shadow region and has the form

$$\phi \sim -\phi_t^{(\mathrm{inc})} \sum_{n=0}^{\infty} \frac{\pi^{\frac{1}{2}} 2^{\frac{1}{6}} \mathrm{e}^{\frac{i\pi}{4}} \mathrm{Ai}'(-\gamma_n^2 \mathrm{e}^{-\frac{2\pi i}{3}})}{\beta^{\frac{1}{3}} (\kappa(0)\kappa(s))^{\frac{1}{6}} \gamma_n^2 \mathrm{Ai}(-\gamma_n^2) \tau^{\frac{1}{2}}} \mathrm{e}^{i\beta^2(s+\tau) - \frac{i\beta^{\frac{2}{3}} \gamma_n^2}{2^{\frac{1}{3}}} \mathrm{e}^{-\frac{2\pi i}{3}} \int_0^s \kappa^{\frac{2}{3}}(s) ds}, \tag{4.39}$$

where τ is the distance along the diffracted ray which leaves the boundary tangentially from the point of arc-length s. The function $\kappa(s)$ is the boundary curvature and $\phi_t^{(\mathrm{inc})}$ is the incident field evaluated in the scaled coordinates at the point of tangency. We note that each term in this sum is exponentially smaller than the one that precedes it.

In terms of a polar angle $\hat{\Theta}$ measured from the focus of the parabola, the boundary can be expressed in the equivalent forms

$$(\hat{X}, \hat{Y}) = \left(\frac{\cos \hat{\Theta}}{2 \sin^2 \frac{1}{2}\hat{\Theta}}, \frac{\sin \hat{\Theta}}{2 \sin^2 \frac{1}{2}\hat{\Theta}} \right), \tag{4.40}$$

or

$$\hat{R} = (\hat{X}^2 + \hat{Y}^2)^{\frac{1}{2}} = \frac{1}{2 \sin^2 \frac{1}{2}\hat{\Theta}}, \tag{4.41}$$

with $\hat{\Theta} = 2\theta_i$ corresponding to the point of tangency. The curvature κ and the arc-length s can then be expressed in terms of $\hat{\Theta}$ as

$$\kappa(s(\hat{\Theta})) = \sin^3 \tfrac{1}{2}\hat{\Theta} \tag{4.42}$$

and

$$s(\hat{\Theta}) = \frac{1}{2} \left(\frac{\cos \frac{1}{2}\hat{\Theta}}{\sin^2 \frac{1}{2}\hat{\Theta}} - \frac{\cos \theta_i}{\sin^2 \theta_i} \right) + \tfrac{1}{2} \ln \left(\frac{\tan \frac{1}{2}\theta_i}{\tan \frac{1}{4}\hat{\Theta}} \right). \tag{4.43}$$

An elementary calculation then shows that $\tau \sim \hat{R} - \frac{\cos \theta}{2 \sin^2 \theta}$ and $\hat{\Theta} \sim 2\theta$, where θ is the angle in the far field directivity introduced in §3, and that, defining the net exponent of ϕ in (4.39) as d_n (including the contribution from $\phi_t^{(\mathrm{inc})}$), then

$$d_n = i\beta^2 R + i \left(\frac{\beta^2}{2} - \frac{\beta^{\frac{2}{3}}}{2^{\frac{1}{3}}} \gamma_n^2 \mathrm{e}^{-\frac{2\pi i}{3}} \right) \ln \left(\frac{\tan \frac{1}{2}\theta_i}{\tan \frac{1}{2}\theta} \right) + \frac{i\beta^2}{2} \cos \theta_i. \tag{4.44}$$

Feeding these results into (4.39) and inverting the scalings reproduces (4.36) precisely (once Φ has been re-expressed in terms of ϕ) and therefore acts as an independent check

https://doi.org/10.1017/S0956792598003441 Published online by Cambridge University Press

on the results. This shows how the diffracted field generated in the shadow for $\beta = O(1)$ changes into a forward-propagating creeping field as $\beta \to \infty$.

The simplest way of analysing the solution in the wedge $\theta_i < \theta < 2\pi - \theta_i$ is to consider the representation of the directivity given by (4.33). In the limit $\beta \to \infty$, we must use the Darwin expansions to replace the ratio of β-dependent differentiated parabolic cylinder functions by an appropriate asymptotic equivalent. This is best achieved by writing $v = -\frac{1}{2} + i\mu$ and then using (B 24). Following a stationary phase and residue treatment, the limiting form of the scattered field $\Phi^{(s)}$ in this region is

$$\Phi^{(s)} \sim \beta \left(\frac{\sin \frac{1}{2}(\theta - \theta_i)}{2r \sin^3 \frac{1}{2}(\theta + \theta_i)} \right)^{\frac{1}{2}} \exp\left(ir - i\beta^2 \frac{\sin \frac{1}{2}(\theta - \theta_i)}{\sin \frac{1}{2}(\theta + \theta_i)} \right). \tag{4.45}$$

This result can also be checked by introducing the scalings leading to (4.37) and (4.38) and solving the appropriate ray problem, a procedure that we have performed but for which we omit the details. It is worth noting from a ray perspective that in the limit $\beta \to \infty$ the expansion fan describing the far-field in the wedge $\theta_i < \theta < 2\pi - \theta_i$ is interpreted as the far-field of a reflected field, whereas for $\beta = 0$ it is viewed very differently, namely as a diffracted field. Our analysis for $\beta = O(1)$ provides a smooth transition between the two.

This now leaves the final region to consider, namely the fully illuminated range $2\pi - \theta_i < \theta < 2\pi$, whose analysis requires the study of (4.27) in the limit $\beta \to \infty$. In this case, the first two terms can be approximated no further but the third can be, since we can set $v_n = -\frac{1}{2} + i\mu_n$ and use (4.34) once more. Doing this yields the scattered field in the form

$$\Phi^{(s)} \sim -e^{ir + \frac{i\pi}{4}} \sqrt{\frac{\pi}{r \sin\theta_i |\sin\theta|}}\, 2^{\frac{1}{6}} \beta^{\frac{2}{3}} \sum_{n=0}^{\infty} \frac{\mathrm{Ai}(-\gamma_n^2 e^{-\frac{2\pi i}{3}})}{\gamma_n^2 \mathrm{Ai}(-\gamma_n^2)} \mathrm{e}^{-\pi\mu_n + i\mu_n \ln\left(\frac{\tan\frac{1}{2}\theta_i}{|\tan\frac{1}{2}\theta|}\right)}. \tag{4.46}$$

The crucial difference between this and its counterpart (4.36) valid in the geometrical shadow is that it is exponentially small by virtue of the $e^{-\pi\mu_n}$ factor. This means that all the superposed modes in (4.46) decay super-exponentially, like $\exp(-\pi\beta^2/2)$ in fact, as $\beta \to \infty$. Our inner diffraction analysis predicts not only a creeping field propagating forwards into the shadow zone, given by (4.36) as $\beta \to \infty$, but also one that propagates backwards into the fully illuminated region; this backward creeping field is exponentially small in the limit $\beta \to \infty$ but is non-negligible for $\beta = O(1)$.

The limit as $\beta \to \infty$ of the directivity $F(\theta)$ is given by

$$F(\theta) \sim -e^{\frac{i\pi}{4} + \frac{i\beta^2}{2}(\cos\theta_i - \cos\theta)} \sqrt{\frac{\pi}{\sin\theta \sin\theta_i}}\, 2^{\frac{1}{6}} \beta^{\frac{2}{3}} \sum_{n=0}^{\infty} \frac{\mathrm{Ai}(-\gamma_n^2 e^{-\frac{2\pi i}{3}})}{\gamma_n^2 \mathrm{Ai}(-\gamma_n^2)} \mathrm{e}^{i\mu_n \ln\left(\frac{\tan\frac{1}{2}\theta_i}{\tan\frac{1}{2}\theta}\right)},$$
$$0 < \theta < \theta_i, \tag{4.47}$$

$$\sim \mathrm{e}^{\frac{i\beta^2}{2}(\cos\theta_i - \cos\theta)} \beta \left(\frac{\sin \frac{1}{2}(\theta - \theta_i)}{2 \sin^3 \frac{1}{2}(\theta + \theta_i)} \right)^{\frac{1}{2}} \exp\left(-i\beta^2 \frac{\sin \frac{1}{2}(\theta - \theta_i)}{\sin \frac{1}{2}(\theta + \theta_i)} \right),$$
$$\theta_i < \theta < 2\pi - \theta_i, \tag{4.48}$$

$$\sim -\mathrm{e}^{\frac{i\beta^2}{2}(\cos\theta_i - \cos\theta) + \frac{i\pi}{4}} \sqrt{\frac{\pi}{\sin\theta_i |\sin\theta|}}\, 2^{\frac{1}{6}} \beta^{\frac{2}{3}} \sum_{n=0}^{\infty} \frac{\mathrm{Ai}(-\gamma_n^2 \mathrm{e}^{-\frac{2\pi i}{3}})}{\gamma_n^2 \mathrm{Ai}(-\gamma_n^2)} \mathrm{e}^{-\pi\mu_n + i\mu_n \ln\left(\frac{\tan\frac{1}{2}\theta_i}{|\tan\theta|}\right)},$$
$$2\pi - \theta_i < \theta < 2\pi. \tag{4.49}$$

https://doi.org/10.1017/S0956792598003441 Published online by Cambridge University Press

4.4.3 *The limit* $\beta \to 0$

In this limit we can expand the β-dependent terms in (4.15) using a Taylor series expansion, which gives

$$\frac{D'_{-1-\nu}(-\bar{p}\beta)}{D'_{-1-\nu}(\bar{p}\beta)} \sim 1 - \frac{2\beta(\nu+\frac{1}{2})\mathrm{e}^{-\frac{i\pi}{4}}\Gamma\left(\frac{1}{2}+\frac{\nu}{2}\right)}{\Gamma\left(1+\frac{\nu}{2}\right)}, \quad \text{as} \quad \beta \to 0. \tag{4.50}$$

To find approximate expressions for the roots, ν_n, of (4.25), we note that

$$D'_{-1-\nu}(0) = -\frac{\sqrt{\pi}2^{-\frac{\nu}{2}}}{\Gamma\left(\frac{1}{2}+\frac{\nu}{2}\right)}, \tag{4.51}$$

which implies that $\nu_n \sim -(2n+1)$. These poles coincide with those from the $\sin(\nu\pi)$ term and this has to be taken in to account when performing the residue calculation. The far-field directivity, in terms of the outer coordinates, can then be written in terms of the diagamma function ψ as

$$F(\theta) \sim \sqrt{\frac{2}{\pi}}\frac{\mathrm{e}^{\frac{i\pi}{4}}\cos\frac{\theta}{2}\sin\frac{\theta_i}{2}}{(\cos\theta-\cos\theta_i)} + \frac{\beta}{\sqrt{2\pi}\sin\frac{\theta_i}{2}\cos\frac{\theta}{2}}\sum_{n=0}^{\infty}\times\frac{\left(\cot\frac{\theta_i}{2}\tan\frac{\theta}{2}\right)^{2n}}{\Gamma(\frac{1}{2}-n)\Gamma(1+n)}$$
$$\times\left[2+(2n+\tfrac{1}{2})\left(2\ln\cot\frac{\theta_i}{2}\tan\frac{\theta}{2}+\psi(\tfrac{1}{2}-n)-\psi(1+n)\right)\right],$$
$$\beta\to 0, \quad 0<\theta<\theta_i, \tag{4.52}$$

$$F(\theta) \sim \mathrm{e}^{\frac{i\pi}{4}}\left(\frac{2}{\pi}\right)^{\frac{1}{2}}\frac{\cos\frac{\theta}{2}\sin\frac{\theta_i}{2}}{(\cos\theta-\cos\theta_i)} - \frac{\beta}{\sqrt{2\pi}\cos\frac{\theta_i}{2}\sin\frac{\theta}{2}}$$
$$\times\sum_{n=0}^{\infty}\frac{\left(-\tan\frac{\theta_i}{2}\cot\frac{\theta}{2}\right)^{n}\left(\frac{1}{2}+n\right)\Gamma\left(\frac{1}{2}+\frac{n}{2}\right)}{\Gamma\left(1+\frac{n}{2}\right)},$$
$$\beta\to 0, \quad \theta_i<\theta<2\pi-\theta_i, \tag{4.53}$$

$$F(\theta) \sim \sqrt{\frac{2}{\pi}}\frac{e^{\frac{i\pi}{4}}\cos\frac{\theta}{2}\sin\frac{\theta_i}{2}}{(\cos\theta-\cos\theta_i)} + \frac{\beta}{\sqrt{2\pi}\sin\frac{\theta_i}{2}\cos\frac{\theta}{2}}\sum_{n=0}^{\infty}\times\frac{\left(\cot\frac{\theta_i}{2}\tan\frac{\theta}{2}\right)^{2n}}{\Gamma(\frac{1}{2}-n)\Gamma(1+n)}$$
$$\times\left[2+(2n+\tfrac{1}{2})\left(2\ln\cot\frac{\theta_i}{2}\tan\frac{\theta}{2}+\psi(\tfrac{1}{2}-n)-\psi(1+n)\right)\right],$$
$$\beta\to 0, 2\pi-\theta_i<\theta<2\pi. \tag{4.54}$$

In each case we observe that ϕ differs from ϕ_s by $O(\beta)$ and for $\beta = 0$ we recover the Sommerfeld result, as required.

https://doi.org/10.1017/S0956792598003441 Published online by Cambridge University Press

4.4.4 *The limits $\theta \to 0$ and $\theta \to 2\pi$*

The limiting behaviour for $F(\theta)$ as $\theta \to 0$ and $\theta \to 2\pi$ for $\beta = O(1)$ follow from (4.29) as

$$F(\theta) \sim -\frac{\sqrt{\pi}\mathrm{e}^{\frac{i\pi}{4}}\mathrm{e}^{\frac{i\beta^2}{2}(\cos\theta_i - 1)}}{2\sqrt{2}\cos\frac{\theta_i}{2}} \frac{\left(\tan\frac{\theta_i}{2}\right)^{\nu_0}\left(\frac{\theta}{2}\right)^{-\nu_0-1}}{\sin\nu_0\pi} \frac{D'_{-1-\nu_0}(-\bar{p}\beta)}{\frac{\partial}{\partial\nu}D'_{-1-\nu}(\bar{p}\beta)|_{\nu=\nu_0}}, \tag{4.55}$$

and

$$F(\theta) \sim -\frac{\sqrt{\pi}\mathrm{e}^{\frac{i\pi}{4}}\mathrm{e}^{\frac{i\beta^2}{2}(\cos\theta_i - 1)}}{2\sqrt{2}\cos\frac{\theta_i}{2}} \frac{\left(\tan\frac{\theta_i}{2}\right)^{\nu_0}\left(\frac{2\pi-\theta}{2}\right)^{-\nu_0-1}}{\sin\nu_0\pi} \frac{\mathrm{e}^{i\nu_0\pi}D'_{-1-\nu_0}(-\bar{p}\beta)}{\frac{\partial}{\partial\nu}D'_{-1-\nu}(\bar{p}\beta)|_{\nu=\nu_0}}, \tag{4.56}$$

respectively; only the first term in each of the series solutions has been included as this dominates. We note that in these limits $F(\theta)$ rapidly oscillates, because ν_0 is complex.

4.5 The limit $\xi \to \infty$, $\eta = O(1)$ for $\beta = O(1)$

We shall need the structure of the field close to the boundary and deep into the shadow region, i.e. as $\xi \to \infty$ with $\eta = O(1)$, since this will be used to match into the creeping field. In this limit the integral solution given by (4.15) becomes

$$\Phi \sim \frac{i\mathrm{e}^{\frac{i\xi^2}{2}}}{2\sqrt{2\pi}} \int_{-\frac{1}{2}-i\infty}^{-\frac{1}{2}+i\infty} \frac{\left(\bar{p}\xi\tan\frac{\theta_i}{2}\right)^{\nu}}{\cos\frac{\theta}{2}} \left[D_{-1-\nu}(-\bar{p}\eta) + \frac{D'_{-1-\nu}(-\bar{p}\beta)}{D'_{-1-\nu}(\bar{p}\beta)}D_{-1-\nu}(\bar{p}\eta)\right] \frac{d\nu}{\sin\nu\pi}. \tag{4.57}$$

This can be evaluated using an arc at infinity in the left-half plane and the residue solution that results is

$$\Phi \sim -\frac{\mathrm{e}^{\frac{i\xi^2}{2}}\sqrt{\pi}}{\sqrt{2}\cos\frac{\theta_i}{2}} \sum_{n=0}^{\infty} \frac{\left(\bar{p}\xi\tan\frac{\theta_i}{2}\right)^{\nu_n}}{\sin\nu_n\pi} D_{-\nu_n-1}(\bar{p}\eta) \frac{D'_{-\nu_n-1}(-\bar{p}\beta)}{\frac{\partial}{\partial\nu}D'_{-\nu-1}(\bar{p}\beta)|_{\nu=\nu_n}}, \tag{4.58}$$

where once more the ν_n are given by (4.25).

4.6 Special cases $\theta_i = 0, \pi$

There are two special cases in which the previous results are not valid, namely $\theta_i = 0$ and π. For the case $\theta_i = 0$, the solution was given by Lamb [27] and is

$$\Phi = D_0(\bar{p}\xi)\left[D_0(p\eta) - \frac{iD'_0(p\beta)}{D'_{-1}(\bar{p}\beta)}D_{-1}(\bar{p}\eta)\right] \tag{4.59}$$

$$= \mathrm{e}^{ix}\left[1 + \frac{\bar{p}\beta}{\bar{p}\beta\sqrt{\frac{\pi}{2}}\mathrm{erfc}(\mathrm{e}^{-\frac{i\pi}{4}}\beta) - 2\mathrm{e}^{i\beta^2}}\sqrt{\frac{\pi}{2}}\mathrm{erfc}\,(\mathrm{e}^{-\frac{i\pi}{4}}\eta)\right]. \tag{4.60}$$

https://doi.org/10.1017/S0956792598003441 Published online by Cambridge University Press

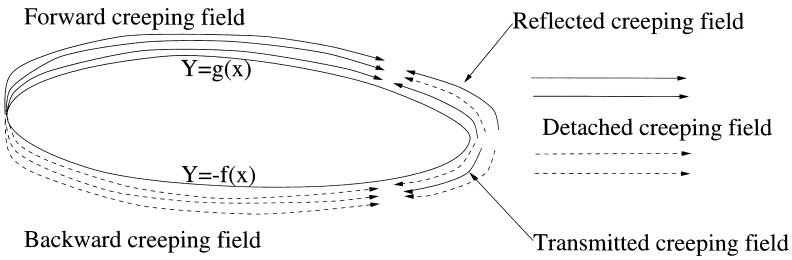

FIGURE 4. Creeping field structure. The forward and backward creeping fields generated at the left tip each propagate to the right tip, where they are partially transmitted, partly reflected and (mainly) radiated into a detached field.

For $\theta_i = \pi$, it is not possible to impose an incoming plane wave when $\beta > 0$. We do, however, note the solution

$$\Phi = \frac{1}{\sqrt{2\pi}} D_\nu(\bar{p}\xi) D_{-1-\nu}(\bar{p}\eta), \tag{4.61}$$

where ν satisfies (4.25), which represents a generalization to $\beta > 0$ of the Sommerfeld solution (4.10); for the root $\nu = \nu_0$ with the largest real part, we have $\nu \to -1$ as $\beta \to 0$.

Conversely, in the limit $\beta \to \infty$ we have $\nu_0 \sim -\frac{1}{2} - i\left(\frac{\beta^2}{2} - \left(\frac{\beta^2}{2}\right)^{\frac{1}{3}} \mathrm{e}^{-\frac{2i\pi}{3}} \gamma_0^2\right)$ where γ_0^2 is the smallest root of $\mathrm{Ai}'(-\gamma^2) = 0$ and (4.61) implies

$$\Phi \sim e^{-\frac{i\pi}{3}} \left(\frac{t_2}{(\eta^2 - \beta^2)(\xi^2 + \beta^2)}\right)^{\frac{1}{4}} \mathrm{Ai}(-t_2^{\frac{2i\pi}{3}}) \mathrm{e}^{\frac{2}{3} i t_1^{\frac{3}{2}}}, \tag{4.62}$$

where $\nu_0 = -\frac{1}{2} - i\mu_0$, so that $\mu_0 \sim \frac{\beta^2}{2} - \left(\frac{\beta^2}{2}\right)^{\frac{1}{3}} \mathrm{e}^{-\frac{2i\pi}{3}} \gamma_0^2$, and for $\eta, \xi = O(\beta)$ we have

$$t_1 = \left[\frac{3\beta^2}{4}\left[\hat{\xi}\sqrt{\hat{\xi}^2 + 1} + \ln(2\hat{\xi})\right] - \frac{3\beta^{\frac{2}{3}} \mathrm{e}^{-\frac{2i\pi}{3}} \gamma_0^2}{2^{\frac{4}{3}}} (\ln(2\hat{\xi}) + \frac{\hat{\xi}}{2\sqrt{\hat{\xi}^2 + 1}})\right]^{\frac{2}{3}}, \tag{4.63}$$

$$t_2 = \left[\frac{3\eta}{4}\sqrt{\eta^2 - \beta^2} - \frac{3\beta^2}{4} \ln\left(\frac{\eta + \sqrt{\eta^2 - \beta^2}}{\beta}\right)\right]^{\frac{2}{3}}, \tag{4.64}$$

where $\xi = \hat{\xi}\beta$.

5 The creeping field

5.1 Introduction

Figure 4 is intended to clarify the nature of the regions to be discussed in this section. Similar fields are produced from the right hand-tip; moreover, each creeping mode repeatedly circulates around the body, shedding most of its energy into a detached field each time it reaches one of the tips.

We shall discuss only the forward case, the backward creeping field (see Figure 4), being very similar in structure. We take $\beta = O(1)$ and define $Y = k^{\frac{1}{2}} y$, writing the upper

https://doi.org/10.1017/S0956792598003441 Published online by Cambridge University Press

part of ∂D as $Y = g(x)$, where $g(0) = g(2a) = 0$, and $2a$ is the length of the body. The analysis which follows assumes that $0 < \theta_i < \pi$; in view of (4.59), the initial and far-field conditions which hold on (5.1)–(5.2) when $\theta_i = 0$ differ from those arising below, the transition between the two cases occurring in a regime in which θ_i is small. We note that the formulation derived below can be significantly simplified in the limits $g \ll 1$ and $g \gg 1$, as is to be expected.

5.2 Forward creeping field

Writing $\phi = \Lambda(k)e^{ikx}v(x, Y)$, where $\Lambda(k)$ will be determined shortly, we obtain at leading order as $k \to \infty$ the parabolic approximation

$$2i\frac{\partial v_0}{\partial x} + \frac{\partial^2 v_0}{\partial Y^2} = 0, \tag{5.1}$$

with boundary condition

$$\frac{\partial v_0}{\partial Y} = i\frac{dg}{dx}v_0, \quad Y = g(x), \tag{5.2}$$

where $v \sim v_0$. The required condition as $Y \to +\infty$ can be regarded as a radiation condition which corresponds to matching into the expansion fan in the 'outer' ray structure (see Figure 2); thus v_0 must have exponential dependence of the form $\exp(iY^2/2x)$ as $Y \to +\infty$ and must not contain terms which are simply algebraic in Y. The initial condition on (5.1) arises from matching as $x \to 0^+$ into the inner (tip) region and we now describe this matching.

We have $g(x) \sim \beta(2x)^{\frac{1}{2}}$ as $x \to 0$ and we solve (5.1) in this limit by seeking a similarity solution of the form

$$v_0 \sim \frac{1}{x^m}\Upsilon\left(\frac{Y}{x^{\frac{1}{2}}}\right) \quad \text{as} \quad x \to 0^+, \tag{5.3}$$

where m remains to be determined. The general solution for $\Upsilon(\zeta)$ is

$$\Upsilon(\zeta) = \mathrm{e}^{\frac{i\zeta^2}{4}}(AD_{2m-1}(\mathrm{e}^{-\frac{i\pi}{4}}\zeta) + BD_{2m-1}(\mathrm{e}^{\frac{3i\pi}{4}}\zeta)). \tag{5.4}$$

The second of these terms does not satisfy the radiation condition, so we require $B = 0$, and the boundary condition on $Y = g(x)$ then implies that $m = -\nu/2$ where ν satisfies (4.25). The similarity exponent m is thus determined by solving an eigenvalue problem, making (5.3) a similarity solution of the second kind. Hence we obtain the initial condition

$$v_0 \sim Ax^{\frac{\nu}{2}}\mathrm{e}^{\frac{iY^2}{4x}}D_{-1-\nu}(\mathrm{e}^{-\frac{i\pi}{4}}Y/x^{\frac{1}{2}}) \quad \text{as} \quad x \to 0 \tag{5.5}$$

for some constant A. Re-expressing (5.5) in inner variables in the limit $\xi \to +\infty$ with $\eta = O(1)$, so that $x = \frac{1}{2}k^{-1}(\xi^2 - \eta^2 + \beta^2) \sim \frac{1}{2}k^{-1}\xi^2$, $y = k^{-1}\eta\xi$, yields

$$\phi \sim A\mathrm{e}^{\frac{i\beta^2}{2}}\Lambda(k)(2k)^{-\frac{\nu}{2}}\xi^{\nu}\mathrm{e}^{\frac{i\xi^2}{2}}D_{-1-\nu}(\bar{p}\eta). \tag{5.6}$$

We require that (5.6) matches with (4.58), and we thus see that each term in (4.58) will generate a creeping mode, with $\Lambda(k) = \Lambda_n(k) = k^{\frac{\nu_n}{2}}$ and where $A = A_n$ can be read off from (4.58). The dominant creeping mode thus corresponds to the root of (4.25) with the largest real part ($\nu = \nu_0$; we note that $\mathrm{Re}\ \nu_0 < -1$ for $\beta > 0$), the other modes having amplitudes which are algebraically smaller in k.

https://doi.org/10.1017/S0956792598003441 Published online by Cambridge University Press

Having determined the initial condition, which completes the specification of v_0, it remains to analyse its behaviour as the other tip, at $x = 2a$, is approached. Taking $g(x) \sim \gamma(2(2a-x))^{\frac{1}{2}}$ as $x \to 2a^-$, the behaviour in the limit $x \to 2a^-$ consists of two regions:

(i) $$Y = O(1), \quad v_0 \sim V(Y), \tag{5.7}$$

where $V(Y) = v_0(2a, Y)$ cannot be determined without solving (5.1), which must be done numerically in general. Since

$$v_0 \sim A\mathrm{e}^{\frac{i\pi}{4}(\nu+1)}x^{-\frac{1}{2}}(Y/x)^{-(\nu+1)}\mathrm{e}^{\frac{iY^2}{2x}} \quad \text{as} \quad Y \to +\infty, \quad \text{for all} \quad x \in (0, 2a), \tag{5.8}$$

this matching outwards into (4.55) when $\nu = \nu_0$, it follows that

$$V(Y) \sim A(2a)^{\nu+\frac{1}{2}}\mathrm{e}^{\frac{i\pi}{4}(\nu+1)}Y^{-(\nu+1)}\mathrm{e}^{\frac{iY^2}{4a}} \quad \text{as} \quad Y \to +\infty. \tag{5.9}$$

(ii) $$Y = O((2a-x)^{\frac{1}{2}}). \tag{5.10}$$

Here we take

$$v_0 \sim \frac{1}{(2a-x)^q}\Omega\left(\frac{Y}{(2a-x)^{\frac{1}{2}}}\right), \tag{5.11}$$

where q will be determined from an eigenvalue problem for $\Omega(\zeta)$, the general solution for which can be written as

$$\Omega(\zeta) = \mathrm{e}^{-\frac{i\zeta^2}{4}}(ED_{-2q}(\mathrm{e}^{-\frac{i\pi}{4}}\zeta) + KD_{-2q}(\mathrm{e}^{\frac{3i\pi}{4}}\zeta)), \tag{5.12}$$

where E and K are constants. The far-field condition on Ω differs from that on Υ; in order to match with (5.7) we require

$$\Omega(\zeta) \sim C\zeta^{-2q}, \quad \text{as} \quad \zeta \to +\infty, \quad V(Y) \sim CY^{-2q} \quad \text{as} \quad y \to 0^+, \tag{5.13}$$

for some constant C whose calculation again requires the numerical solution of (5.1), $\Omega(\zeta)$ being required to contain no terms having exponential dependence of the form $\exp(-i\zeta^2/2)$ as $\zeta \to +\infty$. This implies that $K = 0, E = C$ and the condition on $Y = g(x)$ then requires that q be given by

$$D'_{-1-\rho}(\bar{p}\gamma) = 0, \tag{5.14}$$

(cf. (4.25)) where $q = \frac{1}{2}(\rho+1)$. We thus have

$$v_0 \sim C\mathrm{e}^{-\frac{i\pi}{4}(\rho+1)}(2a-x)^{-\frac{1}{2}(\rho+1)}\mathrm{e}^{-\frac{iY^2}{4(2a-x)}}D_{-1-\rho}\left(\mathrm{e}^{-\frac{i\pi}{4}}\frac{Y}{(2a-x)^{\frac{1}{2}}}\right), \quad \text{as} \quad x \to 2a^-, \tag{5.15}$$

where ρ satisfies (5.14). In general, the behaviour as $x \to 2a$ with $Y = O((2a-x)^{\frac{1}{2}})$ will consist of an infinite number of terms of this type, but that in which the real part of ρ is largest, namely $\rho = \rho_0$ (with $\mathrm{Re}\ \rho_0 < -1$ for $\gamma > 0$), will again dominate.

To obtain matching conditions for the right-hand tip region, we introduce a new set of inner variables (ξ, η), now defined by

$$x = 2a - \frac{1}{2}k^{-1}(\xi^2 - \eta^2 + \gamma^2), \quad y = -k^{-1}\eta\xi. \tag{5.16}$$

From (5.15) we then obtain a matching condition for this inner region, namely

$$\phi \sim k^{\frac{(\nu+\rho+1)}{2}}\mathrm{e}^{2ika}2^{\frac{(\rho+1)}{2}}C\mathrm{e}^{-(\frac{\pi}{4}(\rho+1)+\frac{1}{2}\gamma^2)i}\frac{\mathrm{e}^{-\frac{i\xi^2}{2}}}{(-\xi)^{\rho+1}}D_{-1-\rho}(\bar{p}\eta), \tag{5.17}$$

which gives the incident creeping field in the limit $\xi \to -\infty, \eta = O(1)$.

https://doi.org/10.1017/S0956792598003441 Published online by Cambridge University Press

5.3 Transmitted and reflected creeping fields

Writing

$$\phi = k^{\frac{(\nu+\rho+1)}{2}} \mathrm{e}^{2ika}\psi, \tag{5.18}$$

where we again note that the dominant term is that for which $\nu = \nu_0$, $\rho = \rho_0$, then at the right-hand tip the leading order inner solution for $\xi, \eta = O(1)$ which matches with (5.17) is simply (using (B 5))

$$\psi_0 = cD_\rho(\bar{p}\xi)D_{-1-\rho}(\bar{p}\eta), \tag{5.19}$$

where

$$c = 2^{\rho+1}e^{-(\frac{\pi}{2}(\rho+1)+\frac{1}{2}\gamma^2)i}\Gamma(-\rho)\frac{C}{\sqrt{2\pi}}. \tag{5.20}$$

It is particularly noteworthy that no mode conversion occurs in this region, the solution (5.19) consisting of a single term.

In the limit $\xi \to +\infty$, using (B 4) and (5.19) implies that

$$\psi \sim k^{\frac{\rho}{2}}2^\rho c\,\mathrm{e}^{-(\frac{\pi}{4}\rho+\frac{1}{2}\gamma^2)i}\mathrm{e}^{ik(2a-x)}(2a-x)^{\frac{\rho}{2}}\mathrm{e}^{\frac{iY^2}{4(2a-x)}}D_{-1-\rho}\left(\mathrm{e}^{-\frac{i\pi}{4}}\frac{(-Y)}{(2a-x)^{\frac{1}{2}}}\right), \tag{5.21}$$

holds as matching condition as $x \to 2a^-$, $-Y = O((2a-x)^{\frac{1}{2}})$ (cf. (5.5)), generating a further creeping field along $Y = -f(x)$ from $x = 2a$. In view of (5.18) and (5.21), this transmitted creeping field is a factor $k^{\rho+\frac{1}{2}}$ smaller than the creeping field along $Y = g(x)$ from which it originates.

The expression (5.17) corresponds to the second term in (B 5) in the limit $\xi \to -\infty$ of (5.19); the first term in (B 5) leads to an additional contribution to ψ, which we denote by $\psi^{(r)}$ (the reflected creeping field), for which it follows from (5.19) that

$$\psi^{(r)} \sim k^{\frac{\rho}{2}}2^\rho c\,\mathrm{e}^{(\frac{3\pi}{4}\rho-\frac{1}{2}\gamma^2)i}\mathrm{e}^{ik(2a-x)}(2a-x)^{\frac{\rho}{2}}\mathrm{e}^{\frac{iY^2}{4(2a-x)}}D_{-1-\rho}\left(\mathrm{e}^{-\frac{i\pi}{4}}\frac{Y}{(2a-x)^{\frac{1}{2}}}\right) \tag{5.22}$$

is the matching condition as $x \to 2a^-$, $Y = O((2a-x)^{\frac{1}{2}})$; this reflected creeping field then propagates backwards along $Y = g(x)$ from $x = 2a$. It is also smaller than the original creeping field by a factor $k^{\rho+\frac{1}{2}}$.

The inner solution (5.19) also initiates a further expansion fan propagating into the outer region; by (B 4)–(B 5), ψ_0 has a term in its far-field limit with directivity $c(\cot\frac{1}{2}\theta)^\nu \mathrm{e}^{\frac{i\pi}{4}}/2\sin\frac{1}{2}\theta$.

5.4 Detached creeping field

In $x > 2a$, the leading order detached creeping field, by which we mean the diffracted field shed by the forward propagating creeping field, is given by, using (5.7),

$$2i\frac{\partial v_0}{\partial x} + \frac{\partial^2 v_0}{\partial Y^2} = 0, \tag{5.23a}$$

with

$$\begin{aligned} v_0 &= V(Y), \qquad x = 2a, Y > 0, \\ v_0 &= 0, \qquad x = 2a, Y < 0, \end{aligned} \tag{5.23b}$$

https://doi.org/10.1017/S0956792598003441 Published online by Cambridge University Press

and with radiation conditions holding as $|Y| \to \infty$; a similar problem governs the detached field produced by the backward creeping field. The solution of (5.23*b*) is readily derived in the form

$$v_0 = \frac{1}{(2\pi x)^{\frac{1}{2}}} e^{-\frac{i\pi}{4}} \int_0^\infty V(Y') e^{\frac{i(Y-Y')^2}{2x}} dY'; \tag{5.24}$$

in view of (5.9) this integral has to be interpreted in the appropriate fashion. As $x \to +\infty$ with $Y = O(x)$ we thus obtain the standard asymptotic form

$$v_0 \sim \frac{1}{x^{\frac{1}{2}}} G\left(\frac{Y}{x}\right) e^{\frac{iY^2}{2x}}, \tag{5.25}$$

where in this case

$$G\left(\frac{Y}{x}\right) = \frac{1}{\sqrt{2\pi}} e^{-\frac{i\pi}{4}} \int_0^\infty V(Y') e^{-\frac{iYY'}{x}} dY'. \tag{5.26}$$

The far-field directivity thus features a narrow region $\theta = O(k^{-\frac{1}{2}})$ which contains, through $V(Y)$, complete details of the shape $g(x)$ of the body. This contrasts with diffraction by a blunt body, whose shape within the shadow region makes only an exponentially small contribution to the directivity.

6 Discussion

One of the noteworthy features of our analysis is the identification of a number of new types of creeping and associated diffracted fields (see Figure 4). Creeping field propagation around a two-dimensional body of non-uniform curvature acts in many ways like one-dimensional wave propagation through a non-homogeneous material (an analogy which can be made more precise in the case of an ellipse; see (A 4)); in particular exponentially little reflection occurs away from points at which the curvature of the body is at least $O(k)$. Similar types of creeping field also occur for blunt bodies whose boundaries contain points of non-analyticity; we restrict ourselves to giving a schematic (Figure 5) of the case in which the body contains a corner in the shadow region. The reflected and transmitted creeping fields result from the expansion fan at the corner (cf. Figure 2; the presence of expansion fans underlies many of the creeping field phenomena with which we are concerned) which is produced by the incident creeping field. If the corner coincides with the point of 'tangency' then a backward creeping field of comparable size to the forward one is produced. A corner within the illuminated region also leads to an expansion fan and hence to creeping fields.

A number of natural generalisations of the problem studied here are worth noting:

(a) Other types of tip. While (2.3) is generic, there are other analytical forms whereby $f(x) \sim \beta(2x)^{\frac{1}{2n}}$ for some positive integer n. To obtain the full Helmholtz balance in the tip region the aspect ratio of the body must be changed, with (2.2) being replaced by

$$y = -k^{-(1-\frac{1}{2n})} f(x). \tag{6.1}$$

In consequence, for $n > 1$ the creeping field problem is simpler, because the body appears flat to leading order, but the tip problems are more complicated; in particular, the Helmholtz equation is not separable in the required geometries so that mode conversion

https://doi.org/10.1017/S0956792598003441 Published online by Cambridge University Press

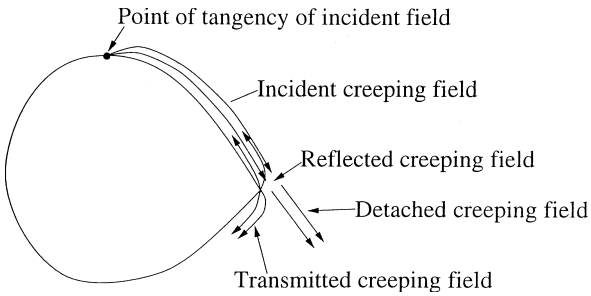

FIGURE 5. Creeping field scattering at a corner.

occurs at the tips. Slender bodies with non-analytic tips, such as cusps and corners of small angle, can also be analysed by similar asymptotic methods.

(b) Three-dimensional problems. The appropriate generalization involves bodies which are slender in one direction only, a thickness of $O(k^{-\frac{1}{2}})$ again being the relevant scaling for such strongly oblate bodies. Similar analyses to those described above still apply but some interesting extra features emerge, particularly with respect to the creeping field.

(c) Implicit in the above analysis is the assumption that the 'centreline' of the slender body is straight. Much of it carries over to the curved case, but obvious complications result from the boundary then not being convex.

It is worth noting the transitions in the far-field behaviour of the scattered field,

$$\phi^{(s)} \sim \frac{1}{r^{\frac{1}{2}}} \Psi(\theta; k) \mathrm{e}^{ikr} \quad \text{as} \quad r \to \infty, \tag{6.2}$$

which occur as the aspect ratio of the scatterer increases. For a body of infinitesimal width, for which the inner problems are of Sommerfeld type, for almost all angles θ we have that the directivity $\Psi = O(k^{-\frac{1}{2}})$, being determined by the field diffracted by the two tips. For $\theta = 2\pi - \theta_i + O(k^{-1})$, however, we have $\Psi = O(k^{\frac{1}{2}})$ due to the reflected field. By contrast, for a body of $O(1)$ aspect ratio we have $\Psi = O(1)$ for almost all θ (due to the reflected field), while $\theta = \theta_i + O(k^{-\frac{1}{3}})$ is a region of rapid variation of the directivity in which $\Psi = O(k^{-\frac{1}{6}})$, determined by matching back into the transition zones mentioned earlier. For bodies of aspect ratio $O(k^{-\frac{1}{2}})$, however, the directivity is rapidly-varying about three different angles, namely where $\theta = 2\pi - \theta_i + O(k^{-1})$ (as above) and where $\theta = O(k^{-\frac{1}{2}})$ and $\theta = \pi + O(k^{-\frac{1}{2}})$, due to the detached creeping fields (albeit with the rapidly-varying component in these cases being algebraically smaller in k than the component due to the field diffracted from the tip). For $\beta \gg 1$ (cf. §4.4.2) then, away from $\theta = \theta_i$ and $\theta = 2\pi - \theta_i$, the diffracted field leads to $\Psi = O(\beta k^{-\frac{1}{2}})$, giving the required transition (an $O(1)$ aspect ratio body has $\beta = O(k^{\frac{1}{2}})$ and the scaling which gives the relevant transition is $\beta = O(1)$). As β becomes large the transition zones emerge out of the diffracted field and correspond to $\theta = \theta_i + O(\beta^{-\frac{2}{3}})$, giving a fourth region of rapid variation in Ψ in this limit and again reproducing the blunt body result for $\beta = O(k^{\frac{1}{2}})$; as $\beta \to \infty$ the field scattered from the tip thus decomposes into, in particular, the reflected field in the illuminated region and transition zones around the shadow region. Finally, we note that the analysis of the reflected field in §3 becomes non-uniform when, taking $f = O(\beta)$, $x \sin\theta_i + y \cos\theta_i = O(1)$ with $x \sin\theta_i - y \cos\theta_i = O(k^{\frac{1}{2}}\beta^{-1})$ for $k^{-\frac{1}{2}} \ll \beta \ll k^{\frac{1}{2}}$ and with $x \sin\theta_i - y \cos\theta_i = O(k)$ for

https://doi.org/10.1017/S0956792598003441 Published online by Cambridge University Press

$\beta = O(k^{-\frac{1}{2}})$ or smaller. In the former case the region of rapid variation in the directivity is $\theta = 2\pi - \theta_i + O(\beta k^{-\frac{1}{2}})$ with $\Psi = O(k^{\frac{1}{4}}\beta^{-\frac{1}{2}})$, again providing the required transition.

We conclude by making the following points by way of summary:

(i) For high-frequency scattering by a convex body, the cases in which the most complicated asymptotic balances result are bodies with aspect ratios of $O(1)$ and $O(k^{-\frac{1}{2}})$. The literature on the former is immense; here we have been concerned with the latter. We emphasize that, while slender, such bodies are nevertheless many wavelengths thick. Moreover, the application of Sommerfeld-type results is not legitimate until the aspect ratio of the body becomes exceedingly small (namely $o(k^{-\frac{1}{2}})$); similar comments may be relevant to the description of other circumstances involving diffraction by thin objects (for example, those involving cracks).

(ii) For aspect ratios of $O(k^{-\frac{1}{2}})$ the inner (tip) problems require the analysis of plane wave scattering by a parabola. We have discussed this in some detail in §4, it having an important status as a canonical diffraction problem, with two of the best-known such problems (Sommerfeld and Fock–Leontovič) as limiting cases. It is thus fortunate that the Helmholtz equation happens to be separable in parabolic cylindrical coordinates.

(iii) Many of the novel phenomena concerning slender bodies relate to the creeping fields. Unlike the situation with blunt bodies, these fields are algebraically (rather than exponentially) small in k; the crucial parameters determining their magnitude are β and γ (the curvatures at the end points), this being quantifiable through the roots of (4.25) and (5.14) with largest real part. Moreover, the creeping fields are confined to boundary layer regions, the analogues of the diffracted rays shed by the creeping rays of blunt body theory emerging from the tips, as expansion fans, rather than from the whole boundary. As a blunt body is made more slender, the transition zones noted in the introduction expand in size to light up the deep shadow region, the field in the shadow becoming of $O(k^{-\frac{1}{2}})$, rather than being exponential small, when the body is made sufficiently slender. The solution (4.61) plays an important role in describing creeping field behaviour and deserves emphasis, being a closed from solution to the full Helmholtz equation which illustrates several noteworthy phenomena (such as as exponentially small backward creeping field in the limit $\beta \to \infty$) and which generalises the $\theta_i = \pi$ Sommerfeld solution.

Acknowledgements

We gratefully acknowledge the support of the EPSRC.

Appendix A Diffraction by an ellipse

A.1 Introduction

Our purpose here is to illustrate some of the preceding analysis by describing certain aspects of the special case in which ∂D is given by the ellipse

$$\frac{(x-a)^2}{a^2} + \frac{y^2}{b^2} = 1, \tag{A 1}$$

with $a > b > 0$. We first briefly consider the order one aspect ratio case and then outline the relevant asymptotic solutions in the slender case $b = O(k^{-\frac{1}{2}})$, $a = O(1)$ for which, in our earlier notation, $\beta = k^{\frac{1}{2}}b/\sqrt{a} = \gamma$. We note that Goodrich & Kazarinoff [35], using

a Green's function approach, have found the approximate surface field for even more slender elliptic cylinders, for which $k^{\frac{1}{2}}b/\sqrt{a} \ll 1$.

A.2 Separable solutions

As is well-known, the Helmholtz equation is separable in elliptic cylindrical coordinates (ξ, η), (see, for example, [4, 36, 37]), where

$$x - a = (a^2 - b^2)^{\frac{1}{2}} \cosh\xi \cos\eta, \quad y = (a^2 - b^2)^{\frac{1}{2}} \sinh\xi \sin\eta, \tag{A 2}$$

the ellipse (A 1) being given by $\xi = \xi_0 \equiv \cosh^{-1}(a/(a^2 - b^2)^{\frac{1}{2}})$; we note that ξ and η here denote different quantities from those elsewhere in the paper. Writing $\phi = \Xi(\xi)\mathscr{H}(\eta)$ yields the Mathieu and modified Mathieu equations

$$\frac{d^2\Xi}{d\xi^2} - k^2(\lambda^2 - (a^2 - b^2)\sinh^2\xi)\Xi = 0, \tag{A 3}$$

$$\frac{d^2\mathscr{H}}{d\eta^2} + k^2(\lambda^2 + (a^2 - b^2)\sin^2\eta)\mathscr{H} = 0, \tag{A 4}$$

where λ is some (complex) constant. There are two useful infinite sum representations for ϕ made up of solutions of this type:

(1) λ chosen such that $\mathscr{H}(\eta)$ is a 2π-periodic function of η;

(2) λ chosen such that $\Xi(\xi)$ satisfies the required boundary condition,

$$\frac{d\Xi}{d\xi} = 0, \quad \xi = \xi_0, \tag{A 5}$$

and a radiation condition at infinity.

The second representation is valid in the shadow region, can be obtained from the first by the Watson transformation followed by a residue calculation (see, for example, [38]) and is the one of interest to us here in describing the creeping field in the limit $k \to \infty$. Thus in case (ii) it follows from (A 3) that as $k \to \infty$ we should introduce the scalings

$$\xi = \xi_0 + k^{-\frac{2}{3}}\hat{\xi}, \quad \lambda \sim (a^2 - b^2)^{\frac{1}{2}} \sinh\xi_0 + k^{-\frac{2}{3}}\hat{\lambda} \tag{A 6}$$

to give at leading order

$$\frac{d^2\Xi_0}{d\hat{\xi}^2} + 2b(a\hat{\xi} - \hat{\lambda})\Xi_0 = 0 \tag{A 7}$$

and the possible values of $\hat{\lambda}$ can, in the usual way, be expressed in terms of the zeros of Ai$'$. The η dependence of each of these creeping modes is then given by (A 4), in which $\lambda = O(1)$ can be determined asymptotically via (A 6). Equation (A 4) could also be viewed as representing one-dimensional wave propagation through a specific type of inhomogeneous medium; as is well-known, in the limit $k \to \infty$ the reflected field in such a medium is exponentially small (see, for example, [36]). This provides an example of the exponentially small nature, noted above, of the 'reflected' creeping field away from regions of high curvature.

In the circular case $a = b$, the corresponding separable solutions are of the form

$$H^{(1)}_{k\lambda}(kr)\Theta(\theta), \tag{A 8}$$

https://doi.org/10.1017/S0956792598003441 Published online by Cambridge University Press

where $x-a=r\cos\theta, y=r\sin\theta$ the possible values of λ are given by

$$H_{k\lambda}^{(1)'}(ka)=0, \tag{A 9}$$

so that $\lambda=1+O(k^{-\frac{2}{3}})$ as $k\to\infty$. Since Θ satisfies

$$\frac{d^2\Theta}{d\theta^2}+k^2\lambda^2\Theta=0, \tag{A 10}$$

the circle acts as a homogeneous (reflectionless) medium for the creeping field. This is to be expected since a circle has constant curvature.

A.3 Slender ellipses

Writing $b=k^{-\frac{1}{2}}\sqrt{a}\beta$, $y=k^{-\frac{1}{2}}Y$, we have

$$g(x)=\beta(x(2a-x)/a)^{\frac{1}{2}} \tag{A 11}$$

and we now discuss the creeping field problem (5.1) in this special case. Somewhat remarkably, for this $g(x)$ the problem admits a similarity solution of the form, (cf. Bluman and Cole [39] for a classification of all classical similarity reductions of the heat equation)

$$v_0=\frac{x^{\frac{\nu}{2}}}{(2a-x)^{(\nu+1)/2}}\mathrm{e}^{-\frac{iY^2(x-a)}{2x(2a-x)}}\Upsilon\left(\frac{a^{\frac{1}{2}}Y}{(x(2a-x))^{\frac{1}{2}}}\right), \tag{A 12}$$

which satisfies the initial-boundary value problem (5.1), (5.5), ν again being a solution to (4.25); it is easily shown that $\Upsilon(\zeta)$ satisfies

$$\frac{d^2\Upsilon}{d\zeta^2}+((2\nu+1)i+\zeta^2)\Upsilon=0, \tag{A 13}$$

$$\frac{d\Upsilon}{d\zeta}=0, \qquad \zeta=\beta, \tag{A 14}$$

with a radiation condition as $\zeta\to+\infty$, and hence, in order to match with (5.5), that

$$\Upsilon(\zeta)=A(2a)^{(\nu+1)/2}D_{-1-\nu}(\bar{p}\zeta). \tag{A 15}$$

In the case of an ellipse, mode conversion therefore does not occur in the creeping field.

It follows from (A 12)–(A 15) that for the ellipse we have

$$V(Y)=CY^{-(\nu+1)}\mathrm{e}^{\frac{iY^2}{4a}} \tag{A 16}$$

and

$$C=A(2a)^{(\nu+1)/2}\mathrm{e}^{\frac{i\pi}{4}(\nu+1)}, \tag{A 17}$$

consistent with our earlier results. In particular we obtain (5.15) as $x\to 2a^-$ with $Y=O((2a-x)^{\frac{1}{2}})$; we note that for the ellipse we have $\gamma=\beta$ so that $\rho=\nu$ here.

Given (A 16), the solution to (5.23*b*) is also of self-similar form, namely

$$v_0=\frac{x^{\frac{\nu}{2}}}{(x-2a)^{(\nu+1)/2}}\mathrm{e}^{\frac{iY^2(x-a)}{2x(x-2a)}}\hat{\Upsilon}\left(\frac{a^{\frac{1}{2}}Y}{(x(x-2a))^{\frac{1}{2}}}\right) \tag{A 18}$$

https://doi.org/10.1017/S0956792598003441 Published online by Cambridge University Press

with, using (B 5),

$$\hat{\Upsilon}(\zeta) = A\left(\frac{a}{\pi}\right)^{\frac{1}{2}} \Gamma(-\nu) D_\nu(-\bar{p}\zeta); \tag{A 19}$$

in (5.25) we thus have

$$G\left(\frac{Y}{x}\right) = \mathrm{e}^{\frac{iaY^2}{2x^2}} \hat{\Upsilon}\left(\frac{a^{\frac{1}{2}} Y}{x}\right). \tag{A 20}$$

Appendix B Useful formulae

What follows is a list of some results concerning parabolic cylinder functions that have been useful in deriving the results contained in the body of this paper. Some are standard and are listed elsewhere [33, 40], whilst others have had to be derived from these.

B.1 Connection formulae

$$D_\nu(z) = \frac{\Gamma(\nu+1)}{\sqrt{2\pi}}\left[\mathrm{e}^{\frac{1}{2}\nu\pi i} D_{-1-\nu}(iz) + \mathrm{e}^{-\frac{1}{2}\nu\pi i} D_{-1-\nu}(-iz)\right] \tag{B 1}$$

$$= \mathrm{e}^{-\nu\pi i} D_\nu(-z) + \frac{\sqrt{2\pi}}{\Gamma(-\nu)} \mathrm{e}^{-\frac{1}{2}(1+\nu)\pi i} D_{-1-\nu}(iz) \tag{B 2}$$

$$= \mathrm{e}^{\nu\pi i} D_\nu(-z) + \frac{\sqrt{2\pi}}{\Gamma(-\nu)} \mathrm{e}^{\frac{1}{2}(1+\nu)\pi i} D_{-1-\nu}(-iz). \tag{B 3}$$

B.2 Asymptotic formulae

Asymptotic expansions valid as $|z| \to \infty$ for $|\nu| = O(1)$ are

$$D_\nu(z) \sim z^\nu \mathrm{e}^{-\frac{1}{4}z^2}, \quad |\arg z| < \frac{\pi}{2}, \tag{B 4}$$

$$D_\nu(z) \sim z^\nu \mathrm{e}^{-\frac{1}{4}z^2} - \frac{\sqrt{2\pi}}{\Gamma(-\nu)} \mathrm{e}^{\nu\pi i} z^{-1-\nu} \mathrm{e}^{\frac{1}{4}z^2}, \quad \frac{\pi}{2} < \arg z < \pi, \tag{B 5}$$

$$D_\nu(z) \sim z^\nu \mathrm{e}^{-\frac{1}{4}z^2} - \frac{\sqrt{2\pi}}{\Gamma(-\nu)} \mathrm{e}^{-\nu\pi i} z^{-1-\nu} \mathrm{e}^{\frac{1}{4}z^2}, \quad -\pi < \arg z < -\frac{\pi}{2}; \tag{B 6}$$

the Stokes lines are at $|\arg z| = \pi/2$ and both exponential terms have been included wherever both are present.

If x, μ are both real and positive then, if $x > 0$ and $\mu \to \infty$, the following uniform expansions hold:

$$D_{-\frac{1}{2}-i\mu}(x\,\mathrm{e}^{-\frac{i\pi}{4}}) \sim 2\sqrt{\pi}\exp\left[-\frac{\pi\mu}{4} - \frac{i\phi_2}{2} + \frac{i\pi}{24}\right]\left(\frac{t_1}{x^2-4\mu}\right)^{\frac{1}{4}} \mathrm{Ai}(-t_1 e^{\frac{2\pi i}{3}}), \tag{B 7}$$

$$D_{-\frac{1}{2}-i\mu}(-x\,\mathrm{e}^{-\frac{i\pi}{4}}) \sim 2\sqrt{\pi}\exp\left[\frac{3\pi\mu}{4} - \frac{i\phi_2}{2} - \frac{i\pi}{8}\right]\left(\frac{t_1}{x^2-4\mu}\right)^{\frac{1}{4}} \mathrm{Ai}(-t_1), \tag{B 8}$$

$$D_{-\frac{1}{2}+i\mu}(x\,\mathrm{e}^{-\frac{i\pi}{4}}) \sim 2\sqrt{\pi}\exp\left[\frac{\pi\mu}{4} + \frac{i\phi_2}{2} + \frac{i\pi}{24}\right]\left(\frac{t_2}{x^2+4\mu}\right)^{\frac{1}{4}} \mathrm{Ai}(-t_2 \mathrm{e}^{\frac{2i\pi}{3}}), \tag{B 9}$$

https://doi.org/10.1017/S0956792598003441 Published online by Cambridge University Press

$$D_{-\frac{1}{2}+i\mu}(-x\,\mathrm{e}^{-\frac{i\pi}{4}}) \sim 2\sqrt{\pi}\exp\left[\frac{\pi\mu}{4}+\frac{i\phi_2}{2}-\frac{i\pi}{8}\right]\left(\frac{t_2}{x^2+4\mu}\right)^{\frac{1}{4}}\mathrm{Ai}(-t_2), \tag{B 10}$$

where

$$t_1 = \begin{cases} -\left[\dfrac{3\mu}{2}\cos^{-1}\left(\dfrac{x}{2\sqrt{\mu}}\right)-\dfrac{3x}{8}\sqrt{4\mu-x^2}\right]^{\frac{2}{3}}, & 2\sqrt{\mu}\geqslant x \\ +\left[\dfrac{3x}{8}\sqrt{x^2-4\mu}-\dfrac{3\mu}{2}\ln\left(\dfrac{x+\sqrt{x^2-4\mu}}{2\sqrt{\mu}}\right)\right]^{\frac{2}{3}}, & 2\sqrt{\mu}\leqslant x, \end{cases} \tag{B 11}$$

$$t_2 = \left[\frac{3\mu}{2}\ln\left(\frac{x+\sqrt{x^2+4\mu}}{2\sqrt{\mu}}\right)+\frac{3x}{8}\sqrt{x^2+4\mu}\right]^{\frac{2}{3}}, \tag{B 12}$$

and

$$\phi_2 = \arg\,\Gamma(\tfrac{1}{2}+i\mu). \tag{B 13}$$

If $x/2\sqrt{\mu}$ is close to 1 then, introducing $\zeta = (2\sqrt{\mu}-x)\mu^{\frac{1}{6}}$, the following expansions hold for $\zeta = O(1), x, \mu \to \infty$, being useful limit cases of (B 7)–(B 8):

$$D_{-\frac{1}{2}-i\mu}(x\,\mathrm{e}^{-\frac{i\pi}{4}}) \sim \sqrt{2\pi}\exp\left[-\frac{\pi\mu}{4}-\frac{i\phi_2}{2}+\frac{i\pi}{24}\right]\mu^{-\frac{1}{12}}\mathrm{Ai}(\zeta\mathrm{e}^{\frac{2\pi i}{3}}), \tag{B 14}$$

$$D_{-\frac{1}{2}-i\mu}(-x\,\mathrm{e}^{-\frac{i\pi}{4}}) \sim \sqrt{2\pi}\exp\left[\frac{3\pi\mu}{4}-\frac{i\phi_2}{2}-\frac{i\pi}{8}\right]\mu^{-\frac{1}{12}}\mathrm{Ai}(\zeta), \tag{B 15}$$

$$D'_{-\frac{1}{2}-i\mu}(x\,\mathrm{e}^{-\frac{i\pi}{4}}) \sim \sqrt{2\pi}\exp\left[-\frac{\pi\mu}{4}-\frac{i\phi_2}{2}-\frac{i\pi}{24}\right]\mu^{\frac{1}{12}}\mathrm{Ai}'(\zeta\mathrm{e}^{\frac{2\pi i}{3}}), \tag{B 16}$$

$$D'_{-\frac{1}{2}-i\mu}(-x\,\mathrm{e}^{-\frac{i\pi}{4}}) \sim \sqrt{2\pi}\exp\left[\frac{3\pi\mu}{4}-\frac{i\phi_2}{2}+\frac{i\pi}{8}\right]\mu^{\frac{1}{12}}\mathrm{Ai}'(\zeta). \tag{B 17}$$

At points at which $\mathrm{Ai}'(\zeta\,\mathrm{e}^{\frac{2\pi i}{3}}) = 0$ we need the representation

$$\frac{\partial}{\partial\mu}D'_{-\frac{1}{2}-i\mu}(x\,\mathrm{e}^{-\frac{i\pi}{4}}) \sim -\sqrt{2\pi}\exp\left[-\frac{\pi\mu}{4}-\frac{i\phi_2}{2}+\frac{7i\pi}{24}\right]\mu^{-\frac{1}{4}}\zeta\mathrm{Ai}(\zeta\,\mathrm{e}^{\frac{2\pi i}{3}}). \tag{B 18}$$

Limiting cases of (B 7)–(B 8), valid as $x, \mu \to \infty$ for $x/2\sqrt{\mu} > 1$, are the Darwin expansions

$$D_{-\frac{1}{2}-i\mu}(\pm x\,\mathrm{e}^{-\frac{i\pi}{4}}) = 2^{-\frac{1}{2}}\exp\left[-\frac{\pi\mu}{4}-\frac{i\phi_2}{2}-\frac{i\pi}{8}\right]\mathrm{E}(\mu,\pm x), \tag{B 19}$$

$$D_{-\frac{1}{2}+i\mu}(\pm x\,\mathrm{e}^{-\frac{i\pi}{4}}) = 2^{-\frac{1}{2}}\exp\left[\frac{\pi\mu}{4}+\frac{i\phi_2}{2}-\frac{i\pi}{8}\right]\mathrm{E}(-\mu,\pm x), \tag{B 20}$$

where

$$\mathrm{E}(\mu,x) \sim 2^{\frac{1}{2}}(x^2-4\mu)^{-\frac{1}{4}}\exp\left(\frac{i\pi}{4}+\frac{ix}{4}\sqrt{x^2-4\mu}-i\mu\ln\left[\frac{x+\sqrt{x^2-4\mu}}{2\sqrt{\mu}}\right]\right), \tag{B 21}$$

$$\mathrm{E}(\mu,-x) \sim 2^{\frac{3}{2}}(x^2-4\mu)^{-\frac{1}{4}}\mathrm{e}^{\pi\mu}\sin\left(\frac{\pi}{4}+\frac{x}{4}\sqrt{x^2-4\mu}-\mu\ln\left[\frac{x+\sqrt{x^2-4\mu}}{2\sqrt{\mu}}\right]\right), \tag{B 22}$$

$$\mathrm{E}(-\mu,\pm x) \sim 2^{\frac{1}{2}}(x^2+4\mu)^{-\frac{1}{4}}\exp\left(\frac{i\pi}{4}+\frac{ix}{4}\sqrt{x^2+4\mu}+i\mu\ln\left[\frac{x+\sqrt{x^2+4\mu}}{2\sqrt{\mu}}\right]\right). \tag{B 23}$$

https://doi.org/10.1017/S0956792598003441 Published online by Cambridge University Press

These results can be used to establish that

$$\frac{D'_{-\frac{1}{2}-i\mu}(-x\,\mathrm{e}^{-\frac{i\pi}{4}})}{D'_{-\frac{1}{2}-i\mu}(x\,\mathrm{e}^{-\frac{i\pi}{4}})} \sim \frac{2ie^{\pi\mu}\cos\left(\frac{\pi}{4}+\frac{x}{4}\sqrt{x^2-4\mu}-\mu\ln\left[\frac{x+\sqrt{x^2-4\mu}}{2\sqrt{\mu}}\right]\right)}{\exp\left(\frac{i\pi}{4}+\frac{ix}{4}\sqrt{x^2-4\mu}-i\mu\ln\left[\frac{x+\sqrt{x^2-4\mu}}{2\sqrt{\mu}}\right]\right)}, \tag{B 24}$$

$$\frac{D'_{-\frac{1}{2}+i\mu}(-x\,\mathrm{e}^{-\frac{i\pi}{4}})}{D'_{-\frac{1}{2}+i\mu}(x\,\mathrm{e}^{-\frac{i\pi}{4}})} \sim \mathrm{e}^{-2i\sqrt{\mu}x}. \tag{B 25}$$

References

[1] Keller, J. B. & Lewis, R. M. (1995) Asymptotic solutions of some diffraction problems. In *Surveys in Applied Mathematics 1*, (ed. J. B. Keller, D. W. McLaughlin and G. C. Papanicolau), pp. 1–82. New York, Plenum Press.

[2] Babič, V. M. & Buldyrev, V. S. (1991) *Short-wavelength Diffraction Theory*. Berlin, Springer-Verlag.

[3] Sommerfeld, A. (1896) Mathematische theorie der diffraction. *Math. Ann.* **47**, 317–374.

[4] Bowman, J. J., Senior, T. B. A. & Uslenghi, P. L. E. (1969) *Electromagnetic and Acoustic Scattering by Simple Shapes*. Amsterdam, North-Holland.

[5] Fock, V. A. (1960) *Electromagnetic Diffraction and Propagation Problems*. New York, Macmillan.

[6] Babič, V. M. & Kirpičnikova, N. Y. (1979) *The Boundary-layer Method in Diffraction Problems*. Berlin, Springer-Verlag.

[7] Tew, R. H., King, J. R., Smith, B. J., Zafarullah, I., Chapman, S. J. & Ockendon, J. R. Scalar wave diffraction by tangent waves. Preprint.

[8] Mei, C. C. & Tuck, E. O. (1980) Forward scattering by a long thin bodies. *SIAM J. Appl. Math.* **39**, 178–191.

[9] Bigg, G. R. (1984) Scattering and the parabolic approximation for slender bodies. *SIAM J. Appl. Math.* **44**, 568–586.

[10] Fedoryuk, M. V. (1981) Scattering of sound waves by a thin acoustically rigid body of revolution. *Sov. Phy. Acoust.* **27**, 336–338.

[11] Valueva, V. N. (1988) Diffraction of plane waves by a slender impedance body of revolution. *Sov. Phy. Acoust.* **34**, 307–308.

[12] Wong, S. K. & Bush, W. B. (1992) Low-frequency acoustic scattering by slender bodies of arbitrary cross section. *J. Acoust. Soc. Am.* **92**, 487–491.

[13] Van Nhieu, M. T. (1988) A singular perturbation problem: Scattering by a slender body. *J. Acoust. Soc. Am.* **83**, 68–73.

[14] Tétyukhin, M. Y. & Fedoryuk, M. V. (1989) Diffraction of a plane sound wave by a slender solid body of revolution in a fluid. *Sov. Phy. Acoust.* **35**, 75–78.

[15] Keller, J. B. & Ahluwalia, D. S. (1971) Diffraction by a curved wire. *SIAM J. Appl. Math.* **20**, 390–405.

[16] Ahluwalia, D. S. & Keller, J. B. (1986) Scattering by a slender body. *SIAM J. Appl. Math.* **80**, 1782–1792.

[17] Geer, J. F. (1978) The scattering of a scalar wave by a slender body of revolution. *SIAM J. Appl. Math.* **34**, 348–370.

[18] Junger, M. C. (1982) Scattering by slender bodies of revolution. *J. Acoust. Soc. Am.* **72**, 1954–1956.

[19] Andronov, I. V. & Bouche, D. (1994) Asymptotic of creeping waves on a strongly prolate body. *Ann Telecomm.* **49**, 205–210.

[20] Ivanov, V. I. (1963) Diffraction of short plane waves on a parabolic cylinder. *USSR Comp. Math. & Math. Phys.* **2**, 255–271.

[21] Newman, E. H. (1990) Plane wave scattering by a material coated parabolic cylinder. *IEEE Trans. Antenn. Prop.* **38**, 541–550.

[22] Rice, S. O. (1954) Diffraction of plane radio waves by a parabolic cylinder. *Bell. Syst. Tech. J.* **33**, 417–504.

[23] Hochstadt, H. (1959) Some diffraction by convex bodies. *Arch. Rat. Mech. Anal.* **3**, 422–438.

[24] Jones, D. S. (1986) *Acoustic and Electromagnetic Waves*. Oxford, Oxford Science Publications.

[25] Ott, R. H. (1985) Scattering by a parabolic cylinder – A uniform asymptotic expansion. *J. Math. Phys.* **26**, 854–860.

[26] Keller, J. B. (1956) Diffraction by a convex cylinder. *IRE. Trans.* **AP-4**, 312–321.

[27] Lamb, H. (1906) On Sommerfeld's diffraction problem; and on reflection by a parabolic mirror. *Proc. Lond. Math. Soc.* **4**, 190–203.

[28] Watson, G. N. (1918) The diffraction of electric waves by the Earth. *Proc. Roy. Soc. Lond.* **A95**, 83–99.

[29] Cherry, T. M. (1949) Expansions in terms of parabolic cylinder functions. *Proc. Edinburgh. Math. Soc.* **8**, 50–65.

[30] Keller, J. B., Lewis, R. M. & Seckler, B. D. (1956) Asymptotic solutions of some diffraction problems. *Comm. Pure & Appl. Math.* **IX**, 207–265.

[31] Whittaker, E. T. & Watson, G. N. (1965) *A Course in Modern Analysis*. Cambridge University Press.

[32] Erdélyi, A., Magnus, W., Oberhettinger, F. & Tricomi, F. G. (1953) *Higher Transcendental Functions, Vol. II*. McGraw-Hill.

[33] Abramowitz, M. & Stegun, I. A. (1972) *Handbook of Mathematical Functions*. Dover.

[34] Chapman, S. J., Lawry, J. M. H., Ockendon, J. R. & Tew, R. H. (1988) On the theory of complex rays. In *Surveys in Applied Mathematics 3*, J. B. Keller, D. W. McLaughlin and G. C. Papanicolau (eds.). New York, Plenum.

[35] Goodrich, R. F. & Kazarinoff, N. D. (1963) Diffraction by thin elliptic cylinders. *Michigan Math. J.* **10**, 105–127.

[36] Berry, M. V. & Mount, K. E. (1972) Semiclassical approximations in wave mechanics. *Rep. Prog. Phys.* **35**, 315–397.

[37] Leppington, F. G. (1967) Creeping waves in the shadow of an elliptic cylinder. *J. Inst. Maths. Applics.* **3**, 388–402.

[38] Levy, B. R. (1960) Diffraction by an elliptic cylinder. *J. Math. Mech.* **9**, 147–159.

[39] Bluman, G. W. & Cole, J. D. (1969) The general similarity solution of the heat equation. *J. Math. Mech.* **18**, 1025–1042.

[40] National Physical Laboratory (1955) *Tables of Weber parabolic cylinder functions*. London, HMSO.